SAPIENZA
UNIVERSITÀ DI ROMA

Multispectral analysis of Nuragic metallic samples (Sardinia, Italy)

Laureando: **Sergio Augusto B. Lins**

Matricola: **1825331**

Relatore: **Giovanni Ettore Gigante**

Correlatore: **Antonio Brunetti**

Facoltà di Scienze Matematiche, Fisiche e Naturali
Corso di laurea in Scienze e Tecnologie per la Conservazione dei Beni Culturali [LM (DM 270/04) - ORDIN

Esame finale anno 2018

A/A 0000/0000

To my mother, my family and my godmother.
I thank all my friends and those who helped me through the last
two years giving me support to keep always moving forward.
To my beloved Virginia, always caring and helpful.

ACKNOLEDGMENTS

First, to God and His guidance, being an anchor during the hardest times.

I would like to thank my supervisors Antonio Brunetti and Giovanni Gigante for the guidance, criticism and opportunity provided for the execution on this work.

I also thank my former supervisor, Joaquim de Assis, who guided me during my bachelor thesis work, for introducing me to this fascinating world of archaeometry.

I also want to express my gratitude to the ARCHMAT consortium for funding the research and trusting my skills and knowledge, giving me a shot of confidence.

Finally, I express my deepest gratitude to all my friends and my family for the emotional and physical support throughout this journey.

"However great and mighty the marvels of nature may seem to us, they are always to be explained by physical reasons. Everything is subordinate to some great law of nature."

- *Jules Verne*

ABSTRACT

In this investigation, a protocol combining the use of Monte Carlo simulations together with energy-dispersive X-ray fluorescence (ED-XRF) analysis was used to determine the chemical composition of a set of nine objects from a private collection, apprehended by *Carabinieri* and without archaeological context. The artefacts are thought to belong to the nuragic period from Sardinia, Italy. The protocol employed is a powerful and non-destructive method useful for cultural heritage applications where usually no sampling is allowed and was applied here with the objective of attesting the authenticity of the objects. The samples were simulated as multilayered structures composed of bulk material and outer corrosion layer so the patina thickness and composition could be estimated as well by the X-ray Monte Carlo (XRMC) package. The method proved useful and powerful, capable of efficiently determining the composition and structure of most of the objects in a total non-destructive approach, attesting the existence of at least one fake in the set. Nevertheless, for a more throughout evaluation and a better estimation of the patina composition, the use of complementary analytical techniques has shown required.

KEYWORDS: archaeometry, XRF, Monte Carlo, bronze, nuragic, Sardinia

LIST OF FIGURES

LIST OF TABLES

INDEX

1 Introduction

Archaeological objects serve as witnesses of the past and their rather uniqueness, turns this category of objects into one of great interest among the scientific community. Analytical approaches towards this category of objects has been carried for a long time, in an attempt to chemically and morphologically characterize them (Alonso et al. 2009; de Caro 2017; Craddock 1976; Kienlin, Bischoff, and Opielka 2006; Meeks 1993; Paparazzo 1994; Pillay et al. 2000; Robbiola, Blengino, and Fiaud 1998). Nevertheless, the removal of fragments for such purposes has become more and more restricted and the approach is now focused in the use of non-destructive techniques always when possible.

X-ray fluorescence (XRF) is a diffused technique and has been used for archaeometric purposes in the past decades since it is non-destructive and yields considerably good results (Guerra 2000; Nørgaard 2017; Pillay et al. 2000). With the advance in technology, XRF has become more and more reliable and the equipment miniaturized, ensuing a greater ease-of-use and portability, making it possible to carry out *in-situ* analysis (Van Grieken and Markowicz 2002).

Although XRF technique allows easily gathering of qualitative information regarding chemical composition, a proper quantitative analysis is still a challenging task. The specific determination of an archaeological metallic alloy is even more difficult (Cesareo et al. 2015), since ancient objects have been buried for extremely long periods of time and, because of that, presents a thick, rough corroded surface, whose chemical composition varies greatly from the original bulk material (Cesareo, Bustamante, et al. 2013; Dillmann et al. 2007; Figueiredo, Araújo, et al. 2013; Ingo et al. 2006; Pronti et al. 2015).

To overcome such difficulties, novelty methods simulating the interaction of X-rays with matter have been developed (Brunetti and Golosio 2014; Schoonjans et al. 2012; Vincze, Janssen, and Adams 1993). More specifically, a combined use of XRF experimental setup with a Monte Carlo algorithm that simulates the X-ray interactions with the sample has been recently used and validated (Bottaini et al. 2018; A. Brunetti, Fabian, et al. 2016; Manso et al. 2015; Schiavon et al. 2016). This protocol takes into full consideration the existence of a

multilayered structure – usually the case for archaeological materials and composed of a combination of surface treatment, incrustations, patina and the bulk. In this way, the protocol adopted can yield reliable data concerning the bulk composition of the material, reflecting the original alloy composition.

Another issue that arises when dealing with ancient objects is their authenticity. Sometimes archaeological findings are prevenient from illegal excavations and therefore presents no historical context, being difficult to attest their originality.

The corroded surface formed throughout the course of thousands of years is difficult to replicate and can be used as a sign of originality of the object (Scott 2002; Selwyn 2004). Moreover, objects obtained through official archaeological expeditions have been characterized and their average alloy composition is known (Atzeni et al. 2005; Craddock 1976; Moravetti et al. 2014; Schiavon et al. 2016). In this context, “unknown” objects can be confronted and a discussion on their authenticity, proposed.

In this work, the combined use of Monte Carlo simulations with an XRF experimental setup and MA-XRF analysis has been put to use in an attempt to attest the authenticity of a group of archaeological bronze objects apprehended by the local police and prevenient from illegal excavations. The set is composed of nine objects thought to belong to the nuragic period in Sardinia, Italy (1500 ~ 500 BC).

2 X-Rays basics

X-rays are defined as an electromagnetic radiation, between γ-rays and ultraviolet radiation possessing energies between 1 KeV and 100 KeV (Cesareo 2000; Van Grieken and Markowicz 2002), being divided into "soft" and "hard" X-rays, according to their energy (Schoonjans 2012). Its classification is somewhat artificial and some authors define X-radiation as residing between 0.15 KeV and 102 KeV, overlapping part of the hard-ultraviolet and soft γ-radiation (Beckhoff et al. 2006).

Developments in technology creating even more efficient detectors throughout the decades has made it possible to detect X- radiation with a very high energy resolution (up to an order of a few hundred electronvolts – eV) (Van Grieken and Markowicz 2002) and making possible the production of ever smaller X-ray spectrometers since its early applications back in the 50's (Ferretti 2000; Guerra 2000).

The most common application of X-ray spectrometry is in quali-quantitative elemental analysis (Nascimento Filho 1999). X-rays interaction with matter can produce radiation, which is intrinsic to each chemical element, and, with the use of a detection system, it is possible to quantify the radiation emitted from the sample and thus identify to which chemical element it belongs, creating an energy continuum spectrum containing the characteristic lines for almost every element within the sample (Ferretti 2000; Van Grieken and Markowicz 2002; Nascimento Filho 1999; Schoonjans 2012). Not every element can be detected, due to their nature; being too light or too heavy and thus being either absorbed by the sample or not detected by the detector, not contributing with a peak on the collected energy spectrum (Barcellos Lins, Humberto Zani, and Teixeira De Assis 2015).

For analytical purposes, spectrometers have been developed throughout time. They consist, in a simplified way, of a source capable of producing X-rays, a sample stage and a detector (Schoonjans 2012; Da Silva 2017). Moreover, optical elements can be added to the source with the purpose of focusing the beam to a micro or nano scale and filters for refining the emitted energy. There are a wide variety of sources and detectors, each with its advantages and disadvantages, which can affect in different manners the energy spectrum

obtained at the end of the analysis (Van Grieken and Markowicz 2002). Nevertheless, other factors can interfere in the spectrum obtained for a particular sample. They comprise, in a general way, the surface and nature of the sample under analysis, geometry between source, sample and detector, and the system efficiency (Brunetti and Golosio 2014; Van Grieken and Markowicz 2002; Nascimento Filho 1999; Schoonjans 2012) and will be briefly discussed in this chapter.

2.1 Interaction with matter

Electromagnetic radiation can interact with matter in different levels: rotational, vibrational and electronic (Callister 2007). X-radiation, being highly energetic, interacts in an electronic level. Upon bombarding a sample surface with a beam of X-rays, three main interactions can occur: Rayleigh scattering, Compton scattering and photoelectric effect (Knoll 2010). Rayleigh scattering is elastic and refers to the scattering of X-rays caused by atomic electrons in which the energy of the scattered photon remains unchanged. Compton scattering refers to the inelastic scattering of X-rays, in which part of the incident photon energy is absorbed by an outer shell electron, recoiling and being thus ejected from the atom. The amount of energy of the scattered photon can be easily calculated by the Compton formula (Van Grieken and Markowicz 2002; Schoonjans 2012).

For analytical purposes, the interaction that raises more interest is the photoelectric effect. This interaction can provide useful information on the composition of a sample and on the relative abundance of its constitutional elements (Ferretti 2000; Nascimento Filho 1999; Schoonjans 2012). The photoionization cross-section (τ) is a function of the atomic number and incident energy, being approximately defined as (Schoonjans 2012):

$$\tau(Z,E) \sim C\frac{Z^4}{E^3} \qquad (1)$$

Photoelectric effect occurs when an incident X-ray photon, with an energy greater than the edge energy (binding energy of an electron in an atomic shell) is fully absorbed by the atom. This process causes the ejection of an electron from the atom, producing a vacancy (Beckhoff et al. 2006; Van Grieken and Markowicz 2002). The produced photoelectron will have an energy equal to the difference between the incident photon and the ejected electron binding energy (Schoonjans 2012). The vacancy thus created can be filled by a transition of a more external electron, belonging to an outer shell, resulting in the production of a photoelectron (Ferretti 2000; Nascimento Filho 1999). The transition can be radiative or non-radiative. If non-radiative, the produced photoelectron will be absorbed by another electron within the atom, generating an Auger electron (or a Coster-Kronig transition, if absorbed by an electron within the same shell) (Schoonjans 2012). If radiative, a characteristic line is produced in an effect called fluorescence. The probability of obtaining a characteristic line instead of an Auger electron is called *fluorescence yield*. In other words, the fluorescence yield is the number of emitted X-ray quanta during the filling of the vacancies divided by the number of initial vacancies (Zschornack 2007).

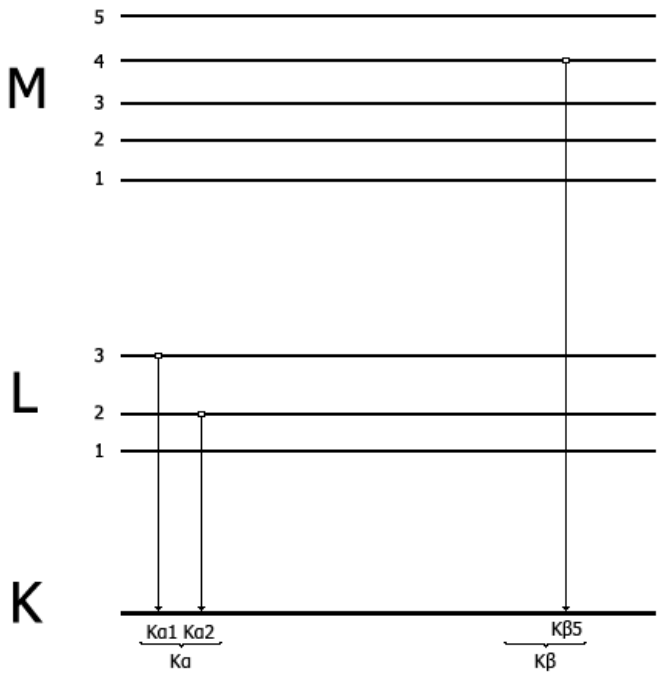

Figure **1** – Simplistic shell transition diagram.

Fluorescence transitions can occur from different shells, e.g. if a vacancy is formed in the K shell of an atom, an electron belonging to shell L or M, and its sub-shells, can fill this vacancy. The energies involved in the transitions are obviously different and will result in detected photons of different energies. If an electron from subshell L_2 occupies the vacancy in shell K, the transition is said to be a KL_2 transition. If it occurs between subshell L_3 and shell K, it is said to be a KL_3 transition. KL transitions emit a radiation named K_α, KM transitions produces K_β radiation. The same is valid for LM and LN transitions, ensuing L_α and L_β radiations, respectively; and analogously valid for other shell transitions. The sub-indexes α and β are, in realty, composed by the several transition possibilities between the shells (e.g. KL_3 and KL_2 producing $K_{\alpha 1}$ and $K_{\alpha 2}$) as it can be seen in Figure 1 (Nascimento Filho 1999). For practical purposes, it is conventional to use the simplified notation referring by K_α the sum of all KL transitions contribution.

That being said, the probability of a characteristic X-ray line being produced, for a given sample, can be quantified and is given by a sum of probabilities: the chance of an incident photon, of energy greater than the threshold for removing an electron from an atom, hits the element Z (photoionization cross-section), the probability of a characteristic line within its series (KL_2, KL_3) is produced and the probability of occurring fluorescence, instead of the production of an Auger electron (*fluorescence yield*) (Nascimento Filho 1999; Schoonjans 2012; Da Silva 2017):

$$Q_{KL_2}(Z,E) = \tau_K(Z,E).F_{KL_2}(Z).\omega_K(Z,E) \qquad (2)$$

2.2 X-rays sources

Radioisotopes are a common source of radiation for medical applications and can also be found on some portable XRF spectrometers (Ferretti 2000; Schoonjans 2012). Radioisotopes, having a proton-rich nucleus, absorbs electrons from its inner shells transforming a proton to a nucleus and creating a vacancy. This vacancy can be filled by a transition from a higher shell electron, producing characteristic X-ray photons (Schoonjans 2012). Nevertheless, the use of radioisotopes requires a series of safety measures; they are time dependent, with short

half-lives and possess lower intensities than photons produced by X-ray tubes, limiting their use (Nascimento Filho 1999; Schoonjans 2012).

The most wide spread mechanism for generating X-rays are the X-ray tubes. Within the tube, a filament is heated by means of an electric current at steady high voltages, which, by thermionic effect, produces electrons (Nascimento Filho 1999). The strong electric field accelerates the electrons towards a target (anode) producing radiation by two simultaneous processes: impact ionization and deceleration (*bremsstrahlung*), which occurs when the electrons lose energy passing through the Coulomb field of a nucleus (Beckhoff et al. 2006; Van Grieken and Markowicz 2002; Schoonjans 2012). The latter provides a continuous spectrum with occasional discrete lines from the anode material, since the electrons may still interact with the anode atoms by photoelectric effect (Van Grieken and Markowicz 2002; Schoonjans 2012). Impact ionization, on the other hand, will cause the ejection of electrons from the inner shells of the anode atoms (if the energy is high enough), creating vacancies. The produced vacancies are filled by electrons from higher shells. If the process is radiative, then characteristic fluorescence lines of the anode atoms will be produced. They are of considerably higher intensity than those produced by *bremsstrahlung* (Schoonjans 2012).

The generated continuum of the X-ray tube is defined within an asymmetrical interval between the emission limits of the source (and detection limits of the system as a whole) being a superposition of the continuous radiation and characteristic lines (Beckhoff et al. 2006; Schoonjans 2012). The total intensity will be proportional to the square of the applied voltage and to the power of one of the atomic number of target atoms (Beckhoff et al. 2006; Van Grieken and Markowicz 2002). In literature, it is possible to find physical models capable of calculating the efficiency of converting electrical power into X-rays (Van Grieken and Markowicz 2002). The efficiency of an X-ray source takes into account several parameters: self-absorption effect, backscattering effects, target material and thickness, voltage, current and age of the equipment, to cite a few (Van Grieken and Markowicz 2002; Schoonjans 2012). These factors are of pristine importance, since a thorough understanding of the excitation spectrum is required in order to perform a proper quantification of the chemical elements present in a sample. If optical elements are used (which is rather common

in modern X-Ray spectrometers), the task is even more challenging. Optical elements have the role of focusing the X-ray beam in narrower areas, making possible the use of techniques such as micro and nano XRF. The efficiency of these elements and how they alter the excitation spectrum are well known (Schoonjans 2012). Nevertheless, the equations that governs these phenomena will not be discussed here, since they are out of the scope of this research.

2.3 X-rays detection

In the past, the detection of X-radiation was done with photographic plates or fluorescent screens, only after being made by means of gas ionization (Beckhoff et al. 2006). In the latter method, ions would move to electrodes with opposite charges, generating current. As it is to expect, these methods were not able to measure the energy of the absorbed radiation, but only its intensity. It was only then, with the development of the proportional counters and later on, the scintillation devices, that the amount of energy of the radiation could be measured (Van Grieken and Markowicz 2002; Schoonjans 2012). Despite their inefficiency compared to modern detectors, proportional counters are still in use due to some advantages: they are very cheap and easy to operate (Beckhoff et al. 2006).

Further on, semiconductors and then silicon drift detectors (SDD) were developed, allowing the detection to be carried at higher resolutions (up to 200 eV or less) (Van Grieken and Markowicz 2002). Semiconductor detectors are still in use, but being slowly replaced by SDD detectors. The latter makes use of low-capacitance charge collector, which results in shorter shaping times and uses a transversal field of ring electrodes that directs the charge carriers towards the collection electrode. This results in significantly higher count rates and devoid them from the need of a bulky nitrogen cooling system, explaining their popularity.

Whereas for semiconducting detectors, the material is doped in a manner that electronic "gaps" are created (p-doping) or an enrichment in electrons is made (n-doping), decreasing the conductivity of the material. The most popular semiconductor detector is the lithium drifted silicon detector (Si(Li)). These detectors relies on the drifting of lithium ions, which

also occurs at room temperature causing a redistribution of the lithium dopants inside the material. For this reason, the detector must be constantly kept under cooling (nitrogen cooling) which makes it bulky and less practical than the Peltier cooled SDD detectors (Beckhoff et al. 2006; Ferretti 2000; Schoonjans 2012).

The detection efficiency of a given detector can be determined by a series of factors and is defined as the amount of photons emitted by the source, which interacts with the sample (if any) and is absorbed by the detector volume. The factors that comprises the detector efficiency are the *geometrical efficiency*, *photopeak efficiency* and *intrinsic efficiency* (Beckhoff et al. 2006; Schoonjans 2012). The problems that arise from the geometrical efficiency, take into account the distance between detector and sample and the limited active area of the detector (Beckhoff et al. 2006).

Whereas for the intrinsic efficiency of a given detector, it can be easily calculated in basis of the detector material and its thickness. The efficiency is given in number of photons that interacts with the detector according to the Beer-Lambert equation (Schoonjans 2012):

$$I = I_0 e^{-\mu(E)\rho w} \qquad (3)$$

Where I is the portion of photons after crossing a sample of density ρ and mass attenuation μ, for a given incident energy E and with thickness w of an incident beam of intensity I_0.

Moreover, the detector window will also absorb some of the incoming radiation. This effect can be as well estimated by the Beer-Lambert equation, and the combination of intrinsic efficiency and window efficiency can be referred to as *quantum efficiency* (Schoonjans 2012).

Photopeak efficiency is rather more complex due to its direct influence on the energy spectrum, comprising the appearance of "artefacts", which can sometimes be misinterpreted as characteristic lines. It can be defined as the ratio of main peak intensity by the total intensity of main peak and its escape peaks, described in the upcoming paragraph.

When the detector absorbs an incoming photon, three main interactions can occur: photoelectric effect, Rayleigh scattering and Compton scattering. The latter two are not much

relevant, since Compton scattering starts causing discrepancies only above 100 KeV and Rayleigh scattering contributions hardly exceeds 10 to 20% of total absorption (Beckhoff et al. 2006). If the incoming photoelectron has an energy higher that the edge energy of Si-K shell (in the case of SDD detectors), the detection process will involve the production of Si-K lines inside the detector volume. The vast majority will be immediately absorbed and will contribute to the collected electrical charge. Nevertheless, there is a possibility that these silicon characteristic lines will escape the detector volume, giving origin to escape peaks, which appears as artefacts on the spectrum (Van Grieken and Markowicz 2002). The energy of the escape peaks is equal to the difference between the incident photoelectron energy and the escape photon energy. This effect is negligible for energies above 10 KeV but, when dealing with lighter elements, this effect plays an important role. Because of that, the escape fraction, i.e. the amount of escape photons, can be calculated and is useful when applying corrections to the spectrum during the quantification step (Schoonjans 2012).

Another effect caused by the action of the detector is the pileup effect, which results in sum peaks within the spectrum. This happens when two photoelectrons enters the detector within a time interval too short for the detector to process them, resulting in a "recognized" signal with an energy corresponding to the sum of the two photoelectrons involved in the process. Sum peaks are hardly misinterpreted as another chemical element, meaning they will not strongly affect a qualitative analysis. In the other hand, for quantitative analysis, the appearance of sum peaks may change the observable abundance of one or other element, making it fundamental to correct this effect, often mathematically. Changing analysis conditions (by the use of filter or lowering the counts per second – cps) can also help counterbalance these effects (Van Grieken and Markowicz 2002; Schoonjans 2012).

There are, of course, other effects that can cause alterations on the spectrum (often hard to quantify). The collection of photons by the detector follows a Gaussian distribution and is a statistical process. The peaks are shown in the spectrum as an approximate Gaussian distribution due to the photon-to-charge conversion that takes place within the detector and the electronic noise caused by the amplification of the signal. An incomplete charge collection can cause disturbances on the lower energy part of the spectrum, representing the

apparent continuum in this region to be higher than expected. This effect is caused by intrinsic defects of the detector such as dead layers and low electric field regions (Schoonjans 2012).

2.4 Quantification methods

When it comes to quantification, the main objective is to convert the obtained spectrum into tangible results, i.e. in values that actually represents the relative abundance of each element within the analyzed sample. In this process, net XRF-line intensities are extracted from the spectrum taking into account the physical interactions involved during the detection process. Only then a quantification is made, involving calibrations and matrix effect correction (Van Grieken and Markowicz 2002; Nascimento Filho 1999).

In usual routine XRF analysis, the energy collected by the detector is between 1 and 30 KeV, hardly surpassing the 30 KeV upper limit. Within this region, self-absorption effect is more intense and should be taken into account (Nascimento Filho 1999). Nevertheless, in the field of archaeometry, the energy limits are pushed forward, comprising higher energies such as 40 or 50 KeV.

Some quantification packages are commercially available. However, they will differ on the basis of the quantitative analysis employed, on the number of standard samples used, spectrometer flexibility and configurations and on the matrix effect correction methods (Van Grieken and Markowicz 2002).

If the sample consists of only a few elements (which is the case of most metallic alloys), and the estimated concentration of each element is known, linear regression method is commonly used for determining each element concentration. Nevertheless, this method requires a considerably high number of standards covering all the combinations of elemental concentrations expected to be found in the sample (Nascimento Filho 1999).

A far more practical method is the Fundamental Parameter Method (FPM). In comparison to the above mentioned method, FPM has the advantage of requiring less standards (roughly one per element expected to be found in the sample). The method requires, however, a

previous knowledge of the physical constants and variables involved in the experimental setup (Nascimento Filho 1999), and relies on describing the fraction of absorbed atoms for a polychromatic X-ray source and a sample composed of various elements (Schoonjans 2012). The concepts involved were briefly discussed on the above sections for a monochromatic beam and homogeneous sample and will be given in more detail here. It is rather easy to approximate the concepts for a more real situation (as required by FPM) (Van Grieken and Markowicz 2002), but the calculations are outside the scope of this research.

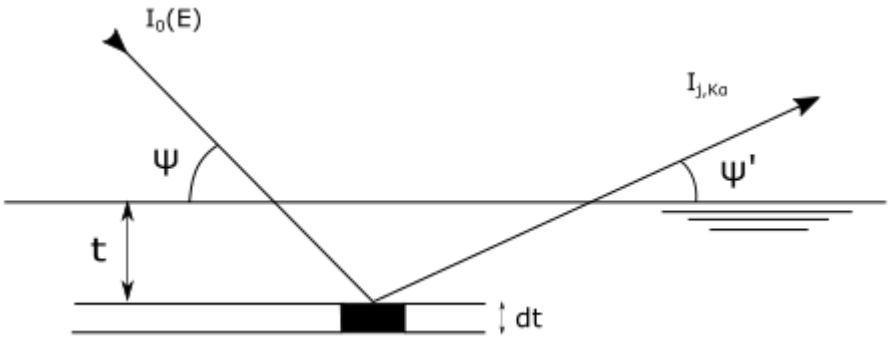

Figure **2** – Schematic drawing representing the mass-attenuation process within the sample.

Take for instance the particular case for a monochromatic beam of energy E and a sample of density ρ_s composed of *n* elements of weight fractions *w* ($\sum_{i=1}^{n} w_i$). The beam reaching the sample will be gradually absorbed undergoing the process of mass-attenuation. The intensity reaching the bulk of the sample at a depth *t* on an infinitesimal part of the sample *dt* (as represented in Figure 2) can be given by the Beer-Lambert equation:

$$I_t(E) = I_0(E)e^{-\mu_s(E)\rho_s t.cossec(\psi)}dt \qquad (4)$$

Where *t*.cossec(ψ) is the total distance travelled by the beam on an incident angle ψ until reaching a depth *t* and $\mu_s(E)$ is the mass attenuation factor for the sample at the energy E, which can be given by the weighted sum of mass attenuation coefficients of each element:

$$\mu_s(E) = \sum_{j=1}^{n} \mu_j(E)w_j \qquad (5)$$

As mentioned on previous sections, the probability of an incident photon yielding a specific line, let us suppose K_α, is equal to $Q_{k_\alpha}(Z,E)$ and depends on the fluorescence yield,

photoionization cross-section and radiative rate. For an element *j* with weight fraction w_j, this is given as: $w_j Q_{k_\alpha,j} \rho_s$. The produced photons will exit the sample and reach the detector under another mass-attenuation process. The photons are scattered in all directions, with only a fraction being emitted towards the detector. This fraction is generally given by Ω/4π, where Ω is small enough to assume that the photons are leaving the sample on a parallel line with the detector at an angle ψ' with the surface. This attenuation can be given in an analogous mode to that of the incident photons, but now with an energy $E_1 = K_\alpha$ energy.

In this manner, the intensity of K_α photons, with energy K_α, produced by the sample, for the element *j* at incident energy E and reaching the detector at an angle ψ' is given as follows:

$$I_{j,K_\alpha} = I_0(E).(Q_{k_\alpha,j}.w_j\rho).\frac{\Omega}{4\pi}e^{-\mu_s(K_\alpha)\rho_s t.cossec(\psi')}e^{-\mu_s(E)\rho_s t.cossec(\psi)}dt \qquad (6)$$

The equation can be re-written as:

$$I_{j,K_\alpha} = I_0(E).(Q_{k_\alpha,j}.w_j\rho).\frac{\Omega}{4\pi}.\exp\left[-\left(\frac{\mu_s(K_\alpha)}{\sin\psi'}+\frac{\mu_s(E)}{\sin\psi}\right)\rho_s t\right]\,dt \qquad (7)$$

Making $\left(\frac{\mu_s(K_\alpha)}{\sin\psi'}+\frac{\mu_s(E)}{\sin\psi}\right)=\chi$, isolating the constants and integrating the equation above from the "bottom" to the surface of the sample (i.e. from 0 to t), it can be re-written as:

$$I_{j,K_\alpha} = I_0(E).(Q_{k_\alpha,j}w_j\rho).G.t.A_{corr} \qquad (8)$$

Where;

$G = \Omega/4\pi$ and $A_{corr} = \left(\frac{1-e^{-\chi\rho T}}{\chi\rho T}\right)$.

A_{corr}, represents the absorption correction term and represents the matrix effects. It has its values between 1 and 0, being approximately 1 for the *infinitely thin* samples.

This approach, for a monochromatic beam and homogeneous sample, considers the production of primary photons only. In order to fit the conditions implied during XRF applications and thus a more realistic approach, when an X-ray tube is used, this concept must be expanded for a polychromatic continuous beam and consider secondary interactions

within the sample. Moreover, to fit the requirements within this work, this method should consider a multi-layered structure and the physical phenomena that comes with it. The existence of corrosion and protective layers on the objects surface, (which is often the occasion for most of the archaeological samples), implies on further mass-attenuation and self-absorption processes. Several papers have been published on the study of multilayered structures and its effects on K_α and K_β emissions (A. Brunetti, Fabian, et al. 2016; Cesareo et al. 2009; Cesareo, De Assis, et al. 2013; Cesareo et al. 2015) and their divergence in composition with the bulk of the object (Condamin and Picon 1964; Debernardi et al. 2017; Nørgaard 2017).

2.5 XRF in cultural heritage

Due to the analytical power provided by X-ray fluorescence (XRF) and its non-destructive characteristics, it has become a standard technique when dealing with cultural heritage objects and precious, timeless artifacts (Bottaini et al. 2017; Buccolieri et al. 2015; Carmona et al. 2010; Nørgaard 2017). The big advantage of yielding the chemical composition of an object, in a fast, rather precise and non-invasive manner is very attractive for most of the researches in the area (Buccolieri et al. 2015; Nørgaard 2017). Since its popularization, XRF has been widely employed on archaeometrical analysis (A. Brunetti, Fabian, et al. 2016; Cesareo, Bustamante, et al. 2013; Comelli et al. 2016; Guerra 2000; Harrison and Howe 2017; Ingo et al. 2013; Manso et al. 2015).

Nowadays XRF is normally used together with several other techniques in order to extract the most of information from the sample as possible. Analytical techniques used together with XRF are Fourier-transform infrared spectrometry (FT-IR), X-rays diffractometry (XRD), scanning electron microscopy (SEM) and Raman spectroscopy, among others (Di Carlo et al. 2017; Schiavon et al. 2013; Scott 2002). These techniques can be complementary to the results obtained from XRF, elucidating the crystalline structure of the material, the different layers that composes the sample and detecting lighter elements (Bottaini et al. 2018; Loureiro et al. 2014), prior “invisible” to routine XRF analysis (Ferretti 2000).

In a general trend, heavier chemical elements "reacts better" with X-radiation in comparison to lighter ones, being easier detected by an XRF spectrometer system. Another point to highlight, as discussed in previous sections, is that X-radiation undergoes attenuation when penetrating the sample. This is important to observe when dealing with corroded metals, since the superficial corrosion layer will interfere with the measurements (A. Brunetti, Fabian, et al. 2016; Schiavon et al. 2013).

Buccolieri et al. (Buccolieri et al. 2015) studied the patina composition of two Riace bronze statues in order to understand the formation of the patinas and give further information for art restorers on how to preserve these priceless objects. The authors made use of a portable XRF spectrometer, which has the obvious advantage of being lightweight and of small size. This feature comes in handy when dealing with objects that cannot leave the museum or their storage place due to a series of reasons. Nevertheless, the equipment proved very useful in handling results. It could properly detect S and Cl, indicators of copper corrosion products such as copper sulfides and copper chlorides, respectively, and other corrosion products such as cuprite. Copper chlorides have four polymorphs and can only be differentiated by X-ray diffractometry, as shown by Di Carlo et al. (Di Carlo et al. 2017). The average composition of the patinas and bronzes could be stablished by the authors and the relative low abundance of certain elements in specific areas of the statues could be attributed to either previous cleaning processes, local restoration procedures or to the deposition conditions the statues were found.

Loureiro et al. (Loureiro et al. 2014) studied the composition of several metallic artefacts found scattered over the archaeological site of *Moinhos de Gola* in Northern Portugal on a quali-quantitative level in order to relate the findings to some archaeological period. The results obtained with μ-XRF analysis proved useful in grouping the objects according to their average composition and ensuing it possible to associate some of them to the Late Bronze Age and some others to the Roman occupation period in the given context. In a similar way, Figueiredo et al. (Figueiredo, Araújo, et al. 2013) studied the composition of 37 metallic objects from *Medronhal* (Portugal) and stablished parallels with other workshops. Nevertheless, other authors, as Nørgaard (Nørgaard 2017), describes the use of XRF as not

enough in distinguishing and characterizing specific workshops or to infer intentional alloying, due to its limitations.

The thickness and nature of the crust formed by corrosion (patina) can differ greatly according to the environmental condition the object was deposited and to its intrinsic properties (Nørgaard 2017; Schiavon et al. 2013, 2016; Scott 2002) Corrosion process can also cause the selective migration of chemical elements within the object, creating a gradient or a re-distribution of the elemental composition as it nears the objects surface (Condamin and Picon 1964; Debernardi et al. 2017). Moreover, past restoration interventions might have been applied to the material, producing the deposition of another layer on the surface of the material (Schiavon et al. 2016; Scott 2002).

Since archaeological samples can rarely be cut for obtaining a cross-section, the precise composition of an archaeological metal is hard to be obtained by conventional XRF spectroscopy – the spectrum would reflect the composition of the surface of the material, as shown by Charalambous et al. (Charalambous, Kassianidou, and Papasavvas 2014). To overcome such difficulties, some authors chose to grind and polish a small surface of the sample with a diamond paste to expose the original surface of the object, and thus perform XRF analysis on that spot (Figueiredo, Araújo, et al. 2013; Schiavon et al. 2013), while others obtain a cross section sample of the object when it is allowed (Harrison and Howe 2017; Loureiro et al. 2014; Quaranta et al. 2014).

These approaches are not the ideal ones when dealing with precious and unique artifacts for a series of reasons. The greater advantage of XRF, as mentioned before, is the ability of obtaining results without interfering in the sample. Moreover, when the original surface of the material is exposed to the atmosphere, it should undergo a local preservation treatment after the analysis, which is often aggressive.

With the objective of overcoming the drawbacks of XRF analysis posed by the existence of one or more superficial layers and without destructively interfering in the sample, a K_α/K_β attenuation model and a computational method based on Monte Carlo simulations were developed and are constantly updated (Brunetti et al. 2004; Brunetti and Golosio 2014;

Cesareo et al. 2009, 2015; Cesareo, De Assis, et al. 2013; Golosio et al. 2014). The Monte Carlo method (XRMC) has already been successfully tested in several archaeological studies (Bottaini et al. 2017, 2018; Brunetti et al. 2015; A. Brunetti, Depalmas, et al. 2016; A. Brunetti, Fabian, et al. 2016; Manso et al. 2015; Schiavon et al. 2016).

3 Monte Carlo simulations

In the following chapter, methods for the simulation of X-radiation interaction with matter, and associated phenomena, will be discussed. Special attention shall be given to the method employed in this research: the XRMC algorithm developed by a group of researchers and contributors from the University of Sassari, Ghent University and the European Synchrotron Radiation Facility, making use of an always up-to-date X-ray interaction cross-section library (*xraylib*). This library contains calculated fundamental parameters such as K-lines, L-lines and several other cross-sections values for all known chemical elements, imperative for the execution of the algorithm.

As described in Chapter 2, X-rays interactions are a rather complex phenomenon. The simulation of probabilities of outcomes, as in classical statistics making use of all variables and parameters, is out-of-hand given the order of magnitude of variables involved. Instead, a more simplistic approach is the use of Monte Carlo (MC) algorithms, which simulates each "run" (or an event) and register the outcome. By "run" (in the particular case of this study), is meant the lifetime of a photon. The outcomes are evaluated when a sufficient number of runs is registered.

There are few packages and toolkits available for the simulation of particle-matter interactions. The majority of these algorithms are, nevertheless, applicable to a large set of particles such as electrons, neutrons and protons and even for hadronic and optical processes, serving as multi-purpose tools operating in a wide energy range. However, when it comes exclusively to X-rays fluorescence interactions, where a more precise and realistic representation of the phenomena is the main goal, computer processing efficiency can be drastically reduced compared to more straightforward algorithms.

Geant4, PENELOPE and MCNP (Monte Carlo N-Particle) codes are some examples of algorithms capable of simulating ED-XRF and are briefly described in the work of Schoonjans, 2012 (Schoonjans 2012). Nevertheless, their drawbacks falls within computing time and processing capabilities, being inconvenient when dealing with a large number of spectra (often the case in culture heritage applications) taking up to several hours of run-time

and (some) lacking the simulation of cascade effects and M-line emissions. Moreover, multi-purpose tools generally make use of rather complex sample and detector geometries, hindering the use of variance-reduction techniques.

A fast and reliable alternative for the afore-mentioned packages was the development of the algorithm used in this work, making use of variance-reduction technique and drastically reducing the run-time to the order of only few minutes. The XRMC algorithm has been validated through several real-world experimental spectra (Bottaini et al. 2017, 2018; A. Brunetti, Depalmas, et al. 2016; A. Brunetti, Fabian, et al. 2016; Brunetti et al. 2015) and with standard reference material (SRM) spectra (Schoonjans et al. 2012).

Van Grieken already proposed in his 2002 handbook of X-ray spectrometry that Monte Carlo simulations can be used as an inverse approach to determine a samples' composition that minimizes the difference between simulated and experimental spectra through a 4-steps protocol. 1 – simulation of the X-ray intensities in the composition range of the unknown; 2 – convolution of the simulated spectra, applying a proper detector response function; 3 – construction of a chi² map as a function of the sample composition; and 4 – interpolation of chi² for the composition corresponding to the minimum (Van Grieken and Markowicz 2002).

3.1 Algorithm overview

It may be difficult to visualize immediately the whole structure and the steps underlined in the execution of such a complex algorithm and how it produces an X-ray fluorescence spectrum. To introduce the reader to the algorithm in a simple and straightforward manner, a first breakdown of the codes' structure can divide the algorithm into three general steps: *input data*, *photon generation* and *output*.

The input data cointains the source parameters, such as energy and excitation spectrum, its geometry and optic parameters. This information is defined according to the experimental setup used, where the exitation spectrum of the equipments' source is recorded and the geometry between source, sample and detector is measured. The source configuration file is not changed during the iteration process, described in item *3.1.2*. The same is valid for the

detector, since the majority of the parameters are “factory dependent” and most of the times provided by the manufacturer.

Other information entered as input data is the sample composition and its physical structure. The algorithm, as aforementioned, simulates the exitation spectrum of a given sample under given conditions. For these matters, the information regarding the sample must be known. This might sound confusing at first, since one of the purposes of the simulations conducted in this work is to estimate the samples’ composition and structure themselves; nonetheless this will be cleared up in the upcoming paragraphs.

Sample information can be summarized in: geometry, shape, phases and composition. Each phase has its own composition, in a way that a multi-layered structured can be generated. The composition comprises the density, atomic number of each present element and their mass percentage.

The photon generation step involves the series of calculations needed to determine the trajectory of the photon and its interaction with the sample. The initial trajectory and energy of the photon are randomly generated within the cone of radiation (simulating the beam produced by the source) using a seed acquired from user input data and local time (when running on Windows OS). This photon can either be terminated before reaching the sample or interact with it. If it reaches the sample, this photon will determine whether the interaction is radiative or non-radiative, and, within the tree, determine the type of atom it interacted with and thereafter in which subshell the interaction occurred. Subsequently, the photon will have its energy and direction updated and will be stored in the pool (virtual multi-channel analyzer – MCA).

A scheme, adapted from Schoonjans et al. (Schoonjans et al. 2012) is shown in Figure 3 below.

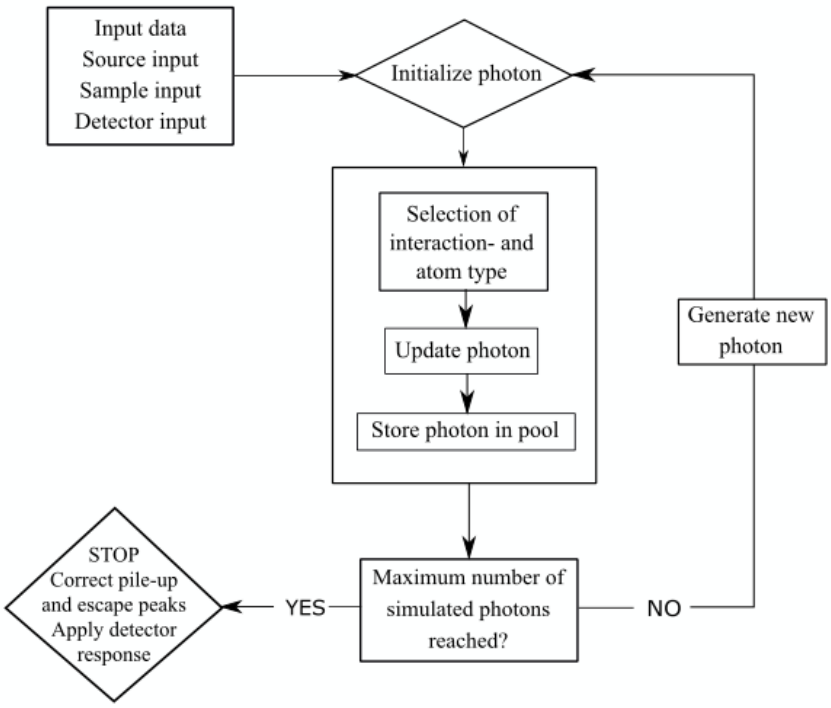

Figure **3** – Block diagram showing in a simplistic way the algorithm structure.

Here, the detection process is "forced" in order to reduce run-time, so the loop that takes place after initializing the photon already considers the photon itself as a "detected" one and will only update its energy and trajectory following the interactions it undergoes until reaching the detector. If the MC program would rigorously follow the general geometry outlines, i.e. strictly simulating the trajectory of the photons escaping from the sample towards the detector and computing only the photons that successively hit it, a successful execution of the code would require an amount of over 100 million simulated photons. To illustrate, in a real case scenario making use of a 30 mm² Si(Li)-detector located about 3 cm from the sample surface, only circa 0.5% of the escaping photons arrive at the detector (Vincze et al. 1993). Nevertheless, the approach adopted here has proven successful, validated with several real-world experimental setups.

When all the photons are terminated, the simulation stops and writes a file containing the spectrum. In this last step, escape and pile-up peaks may be corrected, according to the users' preference, and finally the detector response function is applied.

3.1.1 Classes

During the execution of the algorithm, a variety of *classes* is involved in processing, storing and manipulating the input information. By class, it is meant a C++ object created and used by the algorithm with the purpose of loading parameters from a corresponding file. The program classes are better discussed in Golosio *et al.* (Golosio et al. 2014) work, where the algorithm is presented in full. Here, only the ones of particular interest will be discussed and briefly explained so the reader can better understand the underlying processes.

- *Composition class*

The composition class contains an array of the phases that compose the sample. Each of these phases is considered fully homogeneous and are characterized by their chemical elements and their respective mass percentages. This class stores the sample composition data and is used to calculate the absorption coefficient of each phase, according to the theory presented in Chapter 2.

This class is also accessed when the atom selection step is required by the program, so the photon "choses" the atom it is interacting with in the next interaction process and so forth until the photon is terminated.

- *Quadric, quadricarray and geom3d classes*

In order to simulate the object, it must present a physical volume, delimited and defined as a set of quadric curves, so the simulated photon can interact with the digital sample. The surfaces also define the orientation of the objects surface, separating the outside and inside

of the object. Any defined unitary vector, normal to the objects' surface, will be automatically assumed to have its direction towards the external space.

Geom3d class, in its turn, will compile the written quadric surfaces into one or more objects, accordingly. In the simulations performed, the geometry of the samples was defined as a stack of infinite planes. A series of planes offset in the *z* axis is written within the *quadricarray* file and then compiled into the *geom3d* file to produce a multilayered structure that can properly represent the stratified surface of a real object.

The thickness of the layers (phases) can be easily modified in the *quadricarray* file by simply changing the *z* offset of the quadric planes.

3.1.2 Iteration process

At the given point, the XRMC package is not yet fully automated, requiring time-consuming user intervention to validate the simulated spectra. For the means of estimating a sample structure and composition, the task is even more challenging.

At the end of each execution of the MC code, a spectrum is produced. This spectrum reflects the response of the sample of composition A and geometry B when excited by an X-ray source with known parameters and under known conditions. The simulated spectrum is then superimposed with the experimental one. A confrontation between both spectra is conducted and the data evaluated by the user in order to validate the accuracy between them. If in accordance, i.e. with a sufficiently low difference between experimental and simulated spectra, the input information of the sample is said to be similar enough to the real one. If not, the user updates the composition and geometry of the sample accordingly (now composition A' and geometry B') and execute another run.

A simple scheme to better illustrate the process is shown in Figure 4 below.

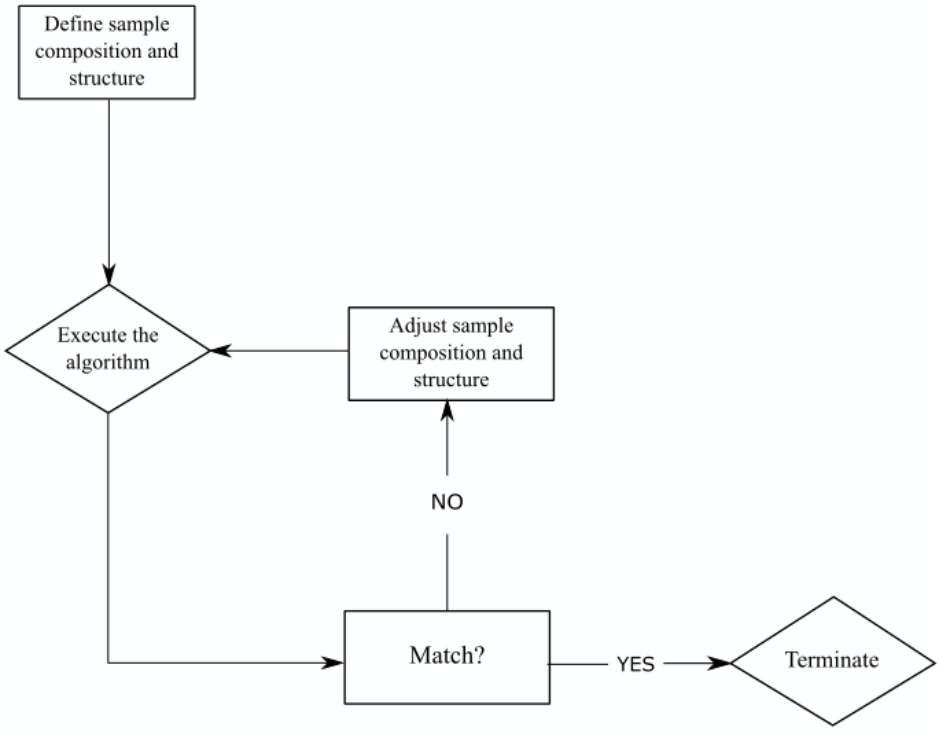

Figure **4** – Block diagram representing the sample composition and structure iteration process.

4 Nuragic Civilization and Ancient Metallurgy

The Nuragic civilization was a mostly pastoral and agricultural society (Becker 1980), which is considered native from the island of Sardinia – located in the Mediterranean basin (Figure 5). The nuragic society can be considered a result of political and economic changes through time, underwent by the indigenous population of Sardinia, and allowed by the use of metals, which made possible their development into a more complex and organized society (Contu 2008; Melis 2003; Minoja, Salis, and Usai 2015).

Figure **5** – Map pinpointing the location of Sardinia island.

This particular civilization flourished between the Early Bronze Age and the Early Iron Age. Some scholars define its existence span as ranging from 1700 BC to 238 BC, ceasing with the advent of the Roman occupation. However, others may suggest that it is not suitable to speak about nuragic civilization past 500 BC and even attribute its origin as early as 1900 BC (Depalmas and Melis 2010; Knapp 1990; Melis 2003; Webster 2014). In literature, it is not uncommon to dedicate a whole chapter just to debate the nuragic chronology, since it is rather confusing and it seems to be no agreement on the topic (Webster 2014).

Without further ado, a brief discussion on the origins and consuetudes of nuragic culture, such as religious practices and metallurgy knowledge will be given in the following sub-sections; in a way that an interpretation can be properly proposed and thoughtfully discussed over the objects studied within this research.

4.1 History, culture and religion

The nuragic people left a large amount of architectural features and objects behind, in a way it is possible to study and try to reconstruct their society in terms of organization, economics and politics (Depalmas and Melis 2010). Unfortunately, there are no written sources, as the nuragic people had no written language. There are, however, some Roman references, which are relatively later to the nuragic period and thus mostly not very helpful (Melis 2003).

It is believed that the nuragic civilization started developing on the Early Bronze Age (EBA) with the appearance of megalithic graves (corridor dolmens) that further evolved into the peculiar "*Tombe dei giganti*" – or giants' tomb –; evolving from individual to collective burials. The nuragic civilization is characterized and named after their particular constructions, the *Nuraghi*, extensively used from around 1500 BC until 500 BC (Balmuth and Tylecote 1976). Nuraghi can be split into proto-nuraghi and tholos nuraghi, each with its distinct architectural features. Tholos nuraghi are the latest manifestation, or form, of these particular fortress-like constructions. Timaeus, an ancient author, already described on the 4th century BC the similarities between the Sardinian nuraghi and the Aegean tholos, associating Mycenaean and Sards for the first time (Becker 1980).

Some of the more complex tholos nuraghi would present fortification walls (antemurals) and secondary towers surrounding the main tower structure, hence the idea that they would serve as fortifications. These typical nuragic constructions have been the source of strong debate in the past concerning its functions. Some authors as Knapp (Knapp 1990) and Taramelli, *aput* Becker 1980 (Becker 1980) attributed a metallurgical function to the nuraghi due to the abundant quantity of copper ingots, both plano-convex ingots and oxhide ingots,

metalworking tools and stone molds found within them. Giardino, *aput* Balmuth 1976 (Balmuth and Tylecote 1976) suggests their use for both metal production as well as for access to and collection of resources. Nowadays it is more acceptable to say that the nuraghi were used for both civil and military functions given its variety in complexity, from a single and simple tower on a top of a hill, to a whole fortification complex with antemurals covering a large area and with the presence of auxiliary turrets (Melis 2003).

Nuraghi were often present within settlements (Melis 2003; Webster 1991), not geographically centered in them, but placed in one extremity of the perimeter, surrounded by stone huts, indicating that the settlement was probably developed on a further time past the construction of the nuraghi. They would act as the fortified residence of an hegemonic family (Webster 1991) – or few of them (Melis 2003) – showing the existence of a certain hierarchical organization. Early settlements usually lacked a common space, except for the nuraghi themselves, "meeting huts" and for the so-called sanctuary villages (Melis 2003), which appeared on a later time.

With the development of the nuragic society, huts were progressively transformed into sector huts, were several other activities started being conducted, e.g. religious (Melis 2003). Non-funerary religious practices (or cults), realized within the villages probably took place during the Late Bronze Age or Early Iron Age, when the settlements reached their full extent (Webster 2014). Within the sector huts, round-shaped rooms – called *rotundas* – composed of a hearth in the center, benches extending thorough the whole perimeter of the room and sometimes with a central water-basin, were unearthed, with characteristics that give rise to an interpretation of their use as for religious purposes (Melis 2003). Before the appearance of dedicated religious sites as the water-temples, *rotundas* and sanctuary villages, the rituals were conducted on burial sites as the giants' tomb (Melis 2003; Webster 2014). Betyls (stone idols) were found within some excavated meeting huts, creating a parallel with betyls found in funerary sites and the slots present on the façade stones of some other burial sites, interpreted by Melis (Melis 2003) as used for holding the small stone betyls.

When it comes to religious practices, the nuragic people had a close relation to water (Melis 2003; Webster 2014). The liquid (drinkable) was scarce in Sardinia and the nuragic

people attributed a "sacred" status to it. Some theories would relate the occurrence of a severe draught in Europe around 1200 BC to have an influence on nuragic architecture and culture, giving rise to the constructions of wells and springs, thus justifying the raise of water status towards a more sacred perspective (Webster 2014). By any means, these theories are rather complex and out of the scope of this research. What is important is that the nuragic people, in fact, did make use of wells and springs as sacred places (Melis 2003), where several bronze miniatures and sculptures – *bronzetti* & *animaletti* – were unearthed (Webster 2014).

The origin of the water-temples as an architectural phenomenon is another whole point of discussion. Due to their intrinsic differences in the execution method, some authors attribute them as non-Sardinian in origin while others vehemently defend their Sardinian origin (Webster 2014). The shape of the main chamber resemble that of the typical *tholos* nuraghi, but the building techniques presented in some temples have no parallel in Sardinia and are completely alien to nuragic culture and civilization (Webster 2014). A common ground is placed on the idea of culture and technological exchange, which might have took place with neighboring societies outside of the island most likely during the Late Bronze Age (13th century BC) (Becker 1980) for sociopolitical reasons or due to the shortage of resources (Knapp 1990). Adding to it, nuragic objects were found at Minoan and Etruscan sites and Phoenician *bronzi* (Webster 2014) and Cypriot copper ingots found at nuragic sites (Atzeni et al. 2005; Balmuth and Tylecote 1976).

Lo Schiavo, *aput* Knapp 1990 (Knapp 1990) suggests that copper production in Sardinia during the Late Bronze Age was probably carried out under teaching and supervision of Eastern metalworkers. Quoting Becker (Becker 1980) on the cultural exchanges in the Mediterranean, mostly focusing on Sardinian relations during the Bronze Age: *"We all recognize that ideas and techniques do diffuse, especially in the context of the complex trade and exchange networks which developed so extensively during the Bronze Age".*

It is hard to neglect that a strong relation between neighboring civilizations took place within central and eastern Mediterranean, involving the exchange of merchandise, knowledge and culture.

4.2 Metallurgy

4.2.1 Ore deposits

For a long time Crete has been taken as the major source of copper in the Mediterranean. In the 70's and 80's (and even before that) archaeologists always debated on the importance and relevance of Sardinia on the metal trade scenario of the Mediterranean basin (Becker 1980). Whether if Sardinia was or was not a center of production is a long and exhaustive discussion. Today, the facts point that Sardinia possibly had abundant sources of copper and native copper available to ancient people and, independent of the origin of the technology and skills employed on the manufacturing of metal objects, it is undeniable that nuragic people did produce several copper, copper-arsenic and bronze artifacts with mastery through its existence (Atzeni et al. 2005).

In this context, metallic ores exploitation in Sardinia can be considered a strong tradition, beginning from ancient times and lasting until the modern age. The remains of mining and metallurgical activities, still seen today, make possible together with geological knowledge, the reconstruction of what would the available ores sources for ancient people be (Atzeni et al. 2005; de Caro 2017).

The well-known copper ore sources, probably exploited by ancient people in Sardinia are pinpointed on Figure 6 below, adapted from Atzeni et al. (Atzeni et al. 2005).

Figure **6** – Ancient copper-ore deposits widespread in Sardinia.

Sardinia is rich in copper and mostly lead ore deposits. The island is also known for its silver deposits (associated to lead, as argentiferous galena) probably known to Romans and Carthaginians at their time (Atzeni et al. 2005). The metallogenic province of Sardinia has a predominance of lead-zinc mineralization, generally accompanied of quartz, barite and fluorite. The earliest exploitation of metals in Sardinia is usually attributed to the *Ozieri* culture, predecessors of the nuragic culture by couple millennia (3500 – 3000 BC) who made use of native copper to produce artefacts (Atzeni et al. 2005).

Tin, as a very important and expensive material at the time, was unlikely to be obtained from the mineralization in Sardinia. Its use is often associated with trade routes in the Mediterranean, which further add to the discussion on cultural and material exchange at the time (Atzeni et al. 2005; Knapp 1990).

Across its territory, substantial amounts of native copper could be found within the ore deposits. Several tons of oxidized copper were also available in ancient times alongside other copper ores such as malachite, azurite, pyrite, chalcopyrite, covellite, chalcocite, enargite and tennantite. For these reasons, typical Sardinian smelted coppers would likely present high quantities (as several ppm's) of bismuth and antimony, as well as reasonably large amounts of lead and several hundreds of ppm's of iron (Atzeni et al. 2005; Balmuth and Tylecote 1976).

Extensive works have been done on tracing the isotopic signature of lead for several ore deposits across the Mediterranean throughout time, making it possible to distinguish the origins of the raw materials employed on the fashioning of copper and bronze artefacts by lead isotopic analysis (LIA) (Attanasio, Bultrini, and Ingo 2001; de Caro 2017).

4.2.2 Technology: the nuragic metalwork

In 1908, at the nuraghe of *Palmavera*, several bronze and copper objects as well as casting tools and slags were unearthed. With this, Taramelli, at his time, suggested that metalworking knowledge from the East was surely imported by nuragic people; for the similarities between the working tools unearthed at Palmavera (and other nuragic sites in Sardinia) with Minoan and Aegean tools was far too much for them to be considered a native Sardinian production (Becker 1980). In anyways, Taramelli ideas reflect an idea of his time, where much attention was given to Cypriot archaeology, while Sardinia archaeology was left in a secondary level of importance (Becker 1980).

Much thought has been put on the origins of copper used by nuragic people, and not until few decades ago, it was quite acceptable that the vast majority of copper was of foreign origin, despite the findings implying the opposite from an archaeological perspective (Atzeni et al. 2005; Balmuth and Tylecote 1976; Becker 1980; Knapp 2000). Knapp (Knapp 1990, 2000) was left astonished by such a thought, since Sardinia, as afore mentioned, was a copper-rich land being very unlikely that nuragic people, having several tons of copper available, would rather import ingots than manufacturing them. This gave the spark needed

to a feverous discussion within the scientific community, where most archaeologists refused to accept the results published by Stos-Gale et al. (1997) (Stos-Gale et al. 1997), which stated that near all copper oxhide ingots from the Mediterranean dating from the 13th century BC onwards were produced in the north of Cyprus.

The controversy on the origin of copper was great despite the availability of analytical techniques since some several decades ago. Scholars were commonly unilateral on the topic, attributing the status of "production center" to one place or another, while, in reality; it is more likely that a large exchange network existed at the time, from the Late Bronze Age onwards, connecting Central and East Mediterranean (Atzeni et al. 2005; Becker 1980).

Nowadays, a common ground can be set around a principle of culture exchange, where several Mediterranean cultures were in contact with one another. Lead isotope analysis, together with other elemental analytic techniques have been increasingly used, evidencing that objects (including copper ingots (Begemann et al. 2001)) from different cultures were indeed traded inter-cultures and thus giving a scientific bias to a cultural exchange theory.

For over four decades, lead isotope analysis (LIA) has been applied to archaeometrical purposes. One of the reasons why, even with the advent of LIA analysis, archaeologists would behave skeptically towards the scientific results, is due to the lack of a normalization or standardization between labs, yielding great fluctuations in the results. Chase, *aput* Becker (1980) (Becker 1980) tried in fact to determine the validity of elemental analysis and has shown that indeed there were great fluctuations in the results, inducing a further distrust upon the scientific methods at the time. To illustrate, it was only less then couple decades ago with the enhancements in technology, mostly in computational processing capabilities and the manufacturing of more precise equipment, that several oxhide ingots were finally accepted to be associated to northern Cypriot mineralization (Atzeni et al. 2005; Moravetti et al. 2014; Stos-Gale et al. 1997).

Even though the majority of oxhide ingots are associated to Cypriot production, the role played by Sardinian people on the Bronze Age Mediterranean metallurgy scenario cannot be diminished. Several archaeological evidences and hoards from different sites spread

throughout the island show Nuragic civilization's outstanding metalworking capabilities. With the sites of Ittireddu, Pattada, Bonnaro, Serra Ilixi, Serra Orrios, Tharos, Ilos and Sorgono (to mention some) summing over tenths of dozens of metal-industry associated objects (Atzeni et al. 2005; Moravetti et al. 2014). Moreover, the nuragic society has a local metalworking culture that precedes them, as the Ozieri culture and the case of the Argaric swords from *di S. Iroxi* (Atzeni et al. 2005), that attest the impossibility of Sardinian swords being imported from El Agar, being thus an authentic Sardinian production.

The artefacts so far unearthed indicates that nuragic people may have shared the same technological level as surrounding contemporary societies (Atzeni et al. 2005). When smelting copper, the use of ground furnaces or more complex and elaborated furnaces (with tuyères) and crucibles was widespread (Atzeni et al. 2005; Gallin and Tykot 1993). The molds were either single-faced or bi-faceted stone molds (Moravetti et al. 2014) or lost-wax molds (Gallin and Tykot 1993). Some thought is also given on the usage of sand molds (Atzeni et al. 2005). The latter is hard to say with certainty, since no archaeological evidence can be found due to the molding condition itself, i.e. the mold is always destroyed after its use.

Copper was used in its "pure" form or alloyed with arsenic or tin. Copper-arsenic alloys were firstly introduced and, on a later time, the use of tin over arsenic became common and widespread (Atzeni et al. 2005). Some scholars affirm that nuragic people used lead as alloying element as well, creating ternary alloys of Cu, Pb and Sn. There are in fact evidences, which supports this line of thought. Lead objects such as clamps for repairing pottery (Atzeni et al. 2005), lead ingots (Moravetti et al. 2014) and the presence of high percentage of lead in bronze artefacts (around 9 wt%) (Schiavon et al. 2016) strongly suggests the intentional use of lead as alloying element. Moreover, analysis performed on crucible fragments from Nuraghe Santa Barbara demonstrate that lead was probably added to bronze to improve its casting properties (Gallin and Tykot 1993).

Begemann et al. (Begemann et al. 2001) investigated almost two decades ago 75 copper and bronze objects, from which 49 are ingots of mixed typologies – oxhide, plano-convex or conical, from the nuragic period in Sardinia. Almost all ingots are of pure copper with few

exceptions containing around 11 wt% of tin and a high content of lead, being interpreted as "ready-to-use" ingots. Some ingots were attributed via LIA to Sardinian origin and "*…are, in every respect, as technically good as any of the oxhide ingots.*"

Regarding the objects (non-ingots) analyzed by Begemann et al., the majority presented low quantities of lead, between 0.01 and 0.74%. LIA analysis pointed that none of the objects possessed a lead signature even remotely similar to that of the analyzed ingots, suggesting that probably the lead was later added to the ingots.

Furthermore, on a more recent perspective, scholars studied the chemical composition of some bronze artifacts from the nuragic period, as the famous "*Cesta*", some *navicelle* models and other objects (Brunetti et al. 2015; A. Brunetti, Depalmas, et al. 2016; Schiavon et al. 2016). The average composition of the objects, taken as originals, is somewhere around 81 wt% Cu, 9 wt% Pb and 8 wt% Sn, plus some other minor elements such as iron (approx. 2 wt%), silver, antimony, arsenic, zinc and titanium (with concentrations inferior to 1 wt%). In contrast, a large collection of Cypriot bronzes from the 11^{th} - 8^{th} centuries BC recently analyzed presented average tin content of 8.1 wt% and only 0.1 to 2.6 wt% of lead (Charalambous et al. 2014). Even though the lead concentration is low, the authors interpreted it as an intentional alloying. From a mechanical perspective it is completely acceptable, since the addition of lead up to 2-3 wt% already improves the fluidity of melted bronze (Charalambous 2016; Ingo et al. 2006).

In the 80's an investigation on the chemical composition of bronze artefacts was conducted over a large number of nuragic artefacts from private collections across Europe (Riederer 1980). The results differ greatly from the aforementioned ones. Tin and lead contents were found to be around 2%, less than a quarter of the value measured in recent studies concerning nuragic artefacts. Nevertheless, these results must be treated with some precaution, since they represent data obtained from private collections, where the authenticity of the objects is not certain.

Iron impurities found within a great deal of nuragic artefacts can be an indicative of the smelting quality or technological level attained by the ancient nuragic metalworkers (Ingo et

al. 2006). Chalcopyrite is one of the most common copper ores and was certainly used in ancient times for extraction of copper (Atzeni et al. 2005). This ore contains iron, which inevitably ends up in the smelted lump of copper. Iron might as well come from the flux used during the smelting process. Nevertheless, the percentage of iron (roughly around 1 wt% for nuragic bronze artefacts – or even Cypriot bronzes (A. Brunetti, Depalmas, et al. 2016; Charalambous et al. 2014; Schiavon et al. 2016)) can attest the efficiency of the smelting process. Percentages around 0.3 wt% are usually associated to a more efficient process, indicating the advanced technological competency and skill of the metalworker (Begemann et al. 2001; Craddock 1976; Ingo et al. 2006).

Lead, as before stated, is commonly present in nuragic artefacts at high quantities. From metallurgical knowledge, it is known that lead and copper are not completely miscible and lead, in such quantities, would precipitate and form another metallic phase (Quaranta et al. 2014), increasing the brittleness of the metal and limiting its usage range (Ingo et al. 2006; Selwyn 2004). This may not seem an issue for religious artefacts or adornments for instance, but it is certainly a limiting factor for tools and weapons, attesting that in order to obtain a high quality tool, the smiths should have at least a minimal knowledge of the influence caused by lead when added together with bronze.

While certain assumptions on the technological level of the smelting process can be done, little or nothing can be inferred on the actual metalworking *techniques* used by nuragic people. To the author's knowledge, there are no reports or publications available so far in literature, which discusses the metalworking techniques on a morphological or metallographic perspective concerning nuragic objects. It is worth saying that there are in fact some mentions about metallographic studies (Atzeni et al. 2005), but on a very superficial level, not getting into any detail on the technology employed for the fashioning and perfecting of the artefacts.

Much is due to the high value of the objects, preventing the execution of any invasive analysis necessary to elucidate these technological questions by any means. If ancient metalworkers in this context cold-worked, annealed, tempered, quenched or altered by any means the final product, it is yet unknown and cannot be discussed beyond speculation.

In anyways, the technology itself involved on the manufacturing of nuragic bronze objects is not the main subject of this research. Albeit, some thought may be given over the subject to help elucidate particular questions imposed throughout the research. Critical factors remains on the composition of the artefacts and its corroded surface, in a way that the objects can be properly characterized and associated – or not – to a nuragic origin.

4.2.3 Corrosion of copper and bronze

Corrosion mechanisms and corrosion products from metallic artefacts are of great importance for, mostly, conservation scientists. Understanding corrosion mechanisms and how the artefacts interacts with the soil and environment, not only in burial contexts, but also during the after-excavation life, is of utmost importance to attest the originality/authenticity of an object, stablish restoration protocols and conservation methods.

Couple books have been published by conservation institutes around the world with a more scientific approach towards metallurgy and electrochemistry, serving as a handful guide to understand corrosion dynamism with metals in a materials science perspective (Scott 2002; Selwyn 2004). Moreover, there are a great deal of publications, which addresses corrosion products whether simply identifying the types of corrosion, its products, conservation protocols or just telling original objects from replicas widely available in literature (Angelini et al. 2014; Bertolotti et al. 2012; Di Carlo et al. 2017; Ingo et al. 2006; Mantovani, Tribaudino, and Facchinetti 2016; Pronti et al. 2015; Robbiola et al. 1998).

In the scope of this research, the understanding of corrosion processes and the identification of its products are of utmost interest. As previously discussed in chapter 2, the corrosion products formed on the surface of corrodible metals will interfere on the measurements performed by XRF, ensuing rather inaccurate results. This limitation can be overcome with the use of the Monte Carlo algorithm described in Chapter 3 and, for those matters, the composition of the corrosion layer(s) – i.e. patina and possible protective layers applied during previous restorations or interventions – must be known or at least estimated to a certain level of accuracy.

Withal the importance of determining some of the corrosion products for a better chemical composition evaluation of the artefacts, this practice can also give insight on the originality of the objects. Long-term corrosion processes are hardly reproducible in laboratory (Quaranta et al. 2014), and thus it is very unlikely that forgeries would be capable of presenting a similar corrosion to that of thousand-year-old artefacts.

Copper, the main alloying element of bronzes, is unstable in its metallic form tending to return to its stable, mineral form, with time. Commonly copper reacts with oxygen and transforms into its oxidized forms: cuprite and tenorite. Other copper corrosion products will comprise copper hydroxychlorides and copper sulfides. Therefore, the most common elements found within the corrosion layers in a copper-alloy (or "pure" copper) artefact would be Sulphur, Chlorine, Oxygen, Copper and the alloying elements – if any.

During the burial and through the course of time, copper alloys undergo a process known as *dealloying*. In this process, the external surface starts reacting with the environment and, by diffusion (since the copper concentration in the surrounding environment is obviously lower than the copper concentration within the artefact) copper will migrate to the surface, altering its composition. The first corrosion product to be formed is cuprite, which further reduces to tenorite (Dillmann et al. 2007). When analyzed under microscope, transversal sections can help easily identify these corrosion products from one another by simply observing the coloration: cuprite is reddish and tenorite is blackish.

Piccardo et al. states in their chapter "Tin and copper oxides in corroded archaeological bronzes" on Corrosion of Metallic Heritage Artefacts: Investigation, Conservation and Prediction of Long Term Behavior (Dillmann et al. 2007) that:

"The understanding of bronze patinas is most often based on two types of corrosion structures […] For both types, an internal tin-enriched layer, often linked to a remnant metallurgical structure of the alloy, is usually evidenced, mainly connected to the presence of oxide compounds containing tin and copper."

Bernard et al. (Bernard and Joiret 2009) found in every object analyzed from a set of bronze artefacts from 800 B.C. Romania and 400 A.D. Morocco that the noble patina always

presents a double layer structure, composed of cuprite and tin oxide (mostly) on the inner part and copper II salts on the outer part.

Tin corrosion products are present in the form of oxides, most commonly tin IV oxides. A certain "protective" factor can be attributed to this particular tin oxide when in the absence of chlorine (Bernard and Joiret 2009).

Copper alloys behave differently according to its composition (bronzes, brass, leaded-bronzes, etc.) and according to the environment they have been buried (Dillmann et al. 2007; Selwyn 2004). High lead contents (around 10 wt%) in bronzes will form segregation products, i.e. lead globules not miscible with the copper matrix that will oxide and, with time be substituted by cuprite through specific mechanisms (Quaranta et al. 2014). Lead corrosion products such as hydrocerrusite may be present as part of the bronze patina as well (Scott 2002).

Precipitation of non-miscible elements (in the form of solid solutions) may occur and create "spots" on the surface of the object, representing a different chemical composition from that average of the object (Bernard and Joiret 2009; Dillmann et al. 2007). One might be careful to avoid such spots in order to get a more accurate result when conducting spot XRF analysis. Albite these spots can also yield relevant information about specific corrosion products and types of corrosion, e.g. pitting, crevice, etc.

When it comes to the mechanisms of corrosion, Pourbaix developed at his time a diagram relating the electric potential and environment pH to corrosion products. The Pourbaix diagram, as it is known nowadays, stablish a relation between the environment and how susceptible it is to oxidize or reduce a group of materials, creating a relation between environment and corrosion products/compounds formed based on the system dynamics (Scott 2002).

Figueiredo et al. and Loureiro et al. (Figueiredo, Silva, et al. 2013; Loureiro et al. 2014) analyzed a set of copper objects belonging probably to the Bronze Age in north Iberian peninsula. The study analyzed corrosion products and types within the samples as well as the

objects chemical composition. The authors detected the formation of cuprite and tenorite in a layered structure as well as inter and transgranular corrosion.

Schiavon et al. (Schiavon et al. 2013) performed a set of analysis with EDXRF and SEM over a group of Iron Age bronze statuettes from southern Portugal, detecting the precipitation of lead as scattered inclusions with globular or interdendritic morphologies in the alloy matrix. The effect is caused by the low miscibility of lead with copper.

Cosano et al. (Cosano et al. 2018) recently studied the corrosion state of a bronze cauldron from Iberian Peninsula Late Iron Age. The authors reported the corrosion state of the artefact and attested the formation of a stratified structure consisting of several mineral phases. Within them, cuprite, cassiterite, malachite, nantokite and atacamite. One analyzed fragment cross-section pointed that the whole object was corroded, showing no traces of the original metallic structure. Moreover, the authors reported that a different corrosion process took place in the inner and outer parts of the artefact, the former being absent of tin, chlorine and sulfur and the latter presenting higher concentrations of carbon, iron and silicon.

Bottaini et al. (Bottaini et al. 2017) characterized by μXRD the corrosion products from a set of ancient bronze objects. All artefacts were covered by a brownish crust and green oxidized corrosion patina. The authors attested the presence of cuprite, malachite, tenorite, brochanite and atacamite as well as the occurrence of quartz and calcite (as soil incrustation derivate). Inclusions rich in lead, bismuth and antimony were also detected.

A more complete list of corrosion products that can arise from a variety of environments and conditions is available in literature (Scott 2002; Selwyn 2004). Nevertheless, corrosion products can be easily identified with a range of analytical techniques up to a satisfactory level. That being said, an estimation of the corrosion products (the most common chemical elements) deposited on the surface of bronze artefacts can be performed – or even guessed by the surface color –, making XRMC technique a powerful tool for identifying the chemical composition of corroded objects without requiring any invasive protocol.

5 Materials and Methods

In this section, the artefacts analyzed and the following techniques used for these matters will be presented and discussed.

5.1 Materials

The analyzed set of objects consists of nine artefacts made of tin-bronze, leaded bronze or lead. All of them are believed to be of Nuragic origin and are out of archaeological context. The objects are part of a large batch of over 430 pieces apprehended by *Carabinieri* and obtained from illegal excavations. They are now in possession of the *Soprintendenza Archeologia, belle arti e paesaggio per le province di Sassari e Nuoro,* which kindly provided the objects for investigation.

Among the analyzed objects, there are *bronzetti*, daggers, a small double axe and a *navicella*. A full list of the objects and their descriptions can be found in Annex A and an illustration is depicted in Figure 7 below.

Figure **7** – Set of analyzed objects. 1-3 – Daggers (42, 43 and 44), 4-5 – *Bronzetti* (47 and 52), 6 – Navicella, 7 – Double axe "*axe-adze*", 8 – Axe, 9 – Boat (*navicella*) head.

5.2 Characterization

The objects were evaluated by means of X-ray fluorescence analysis and a Monte Carlo protocol. The adopted protocol involves the concomitant use of XRF measurements and Monte Carlo simulations. The approach is based in comparing simulated spectra with experimental spectra, updating the sample composition and structure to minimize the difference between them.

One of the samples, namely axe nº 111, was analyzed by Macro X-ray fluorescence (MA-XRF), yielding a useful elemental map to better understand the corrosion products and better describe the sample structure, minimizing the error in MC simulations.

5.2.1 XRF in-situ analysis

All XRF analysis were conducted within the *Soprintendenza Archeologia, belle arti e paesaggio per le province di Sassari e Nuoro* facilities, where the samples are stored.

The spectrometer used was an ELIO model spectrometer from XG-Lab, equipped with a 25 mm² active area Silicon Drift Detector (SDD) with a 12 μm Be window and resolution down to 135 eV at Mn Kα energy. The spectrometer's source is an Rh anode with operation conditions ranging from 10 to 50 KV and 5 μA to 200 μA. Collimation diameter is 1 mm. For the analysis, tube voltage and current were set to 40 KV and 60 μA respectively. Acquisition time was of 60 seconds. Figure 8 illustrates the experimental setup.

Each sample was analyzed in at least two different spots in order to obtain a more reliable result, which can better represent the chemical composition of the sample as a whole, and provide a statically good set of spectra.

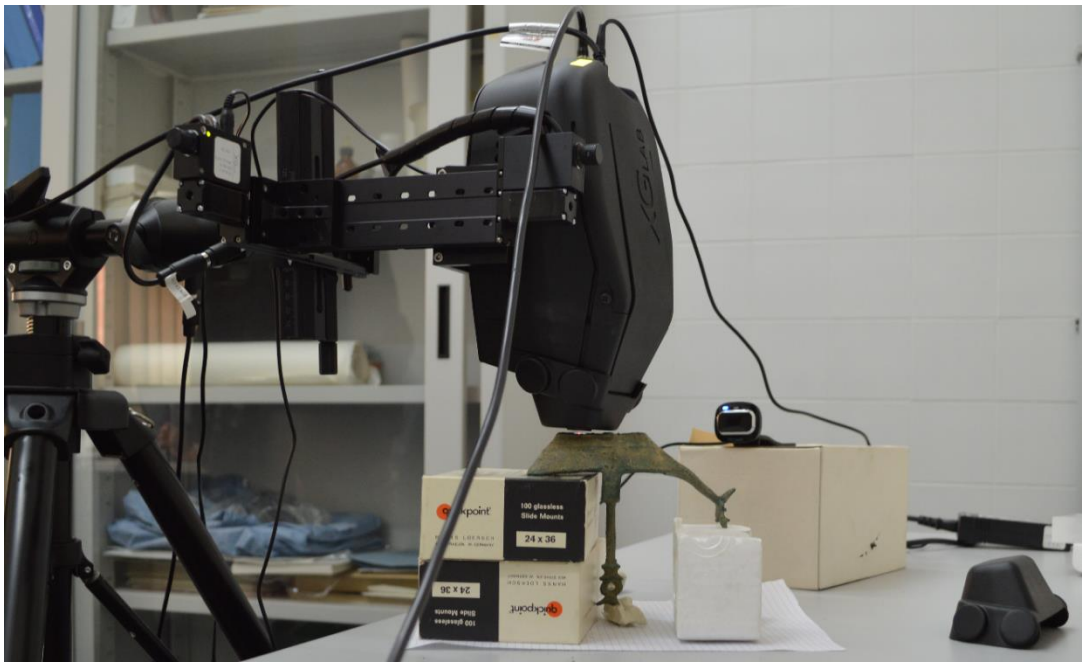

Figure **8** – Experimental setup at *Soprintendenza Archeologia, belle arti e paesaggio per le province di Sassari e Nuoro.*

5.2.2 MA-XRF analysis

In collaboration with *Porto Conte Ricerche*, a Tornado M4 spectrometer from Bruker was used to create the elemental map of sample's 111 surface. This state-of-the-art spectrometer houses two Rh anode tubes (one collimated and another with polycapillary lenses) capable of operating at up to 50KV and two SDD detectors of 30 mm² active area each with an energy resolution down to 145 eV at 300 Kcps.

The tube used for the elemental map acquisition was the collimated one, and the conditions were set to 50 KV and 30 μA. Analysis was carried under a vacuum atmosphere. Data acquisition time was of one hour and twenty-seven minutes. The analyzed area was of 14 x 8 mm with a total of 7000 points measured during the process.

5.2.3 Monte Carlo Simulations

Finally, Monte Carlo protocols yielded the results concerning sample composition and structure. The process comprised evaluating the XRF data gathered by *in-situ* analysis together with the simulated spectra produced by the XRMC package, described in Chapter 3.

Upon a first qualitative analysis of the measured spectrum, the initial "guess" of the structure and composition of the sample was made. With the use of a spreadsheet containing a small database with the most common corrosion products for copper, zinc, tin and lead, and based on the color presented by the objects' surface, the starting patina composition of the sample could be estimated as well. Composition and structure were iteratively adjusted to better fit the measured spectrum. Comparison between spectra was first done visually; further, chi-squared tests were performed to finely adjust them.

Since there is an inherent difference in the number of MCA channels between the virtual MCA and the equipment's MCA (1000 channels for the former and 4096 for the latter), the chi-squared test could not be performed on the go. For these matters, a short code was written in python. To make the comparison, the experimental spectrum was translated into a 2x1000 vector containing the energies and corresponding counts as close as possible to the energy values generated within the simulation. With both spectra now presenting the same length, the test was run computing the squared root from the squared difference of each point and dividing by the number of computed points.

To illustrate, suppose the below described vectors containing the KeV energies of, first the simulated spectrum and then the measured one. It is clear that not every point from the measured spectrum has a corresponding one with the simulated spectrum. Therefore, the measured spectrum is translated, carrying only the closest corresponding KeV values that exist within the simulated spectrum.

Sim_KeV (0, 0.04, 0.08, 0.12, 0.16, …, 40)

Meas_KeV (0.0050, 0.0169, 0.0287, 0.0406, 0.0524, 0.0761, 0.0879, 0.0998, 0.1116, 0.1235, 0.1353, 0.1472, 0.1590, 0.1708, 0.1827, …, 40)

Trans_KeV (0.0050, 0.0406, 0.0761, 0.1235, 0.1590, …, 40)

The chi-squared test algorithm is presented in full in Annex B.

The XRMC package ran on a Dell XPS 14 L421X laptop (3rd-generation Intel Core i7-3537U, 8 GB DDR3 SDRAM) running on Windows 10. Each run took approximately 6 minutes varying according to the complexity of the sample structure. The spectra were compared and processed with a graphics analysis software.

6 Results and discussions

In the following section, all the results relevant for stablishing a proper discussion and interpretation of the analyzed artefacts will be presented. The discussion is structured in topics regarding each particular object or a set of objects that shares similar features. Moreover, following the proposed goal of the investigation, the results herein presented will establish a dialog to ascertain the legitimacy of the artefacts and to validate the adopted Monte Carlo protocol.

A summary containing the complete elemental composition, patina thickness and chi² test for the XRMC simulations from all analyzed artefacts is presented in Annex C. To introduce the results more objectively, each objects' – or set of objects – discussion in this chapter will be provided with its corresponding extract from Annex C.

- *Daggers 42 and 43*

This couple of dagger blades present similar features to daggers from *Pirosu-Su Benatzu* and *Su Monte* (which belong to somewhere between the 12th and 8th centuries BC) (Atzeni et al. 2005; Moravetti et al. 2014). Dagger 42 is compatible in dimension and shape with some authentic nuragic daggers, with length between 15 and 20 cm and 4.4 and 6.2 cm in width, being only slightly smaller. The dagger also shares the same elongated central ribbing found in other authentic daggers. Dagger 43 is considerably smaller than average daggers of similar type and presents a rounder shape, being more similar to a dagger from *Complesso nuragico di Albini* (Moravetti et al. 2014).

The Monte Carlo protocol was applied over a set of four different XRF spectra from Dagger's 42 surface and three spectra from Dagger 43. The results are presented in Table 1 below and a comparison between simulated and measured spectra is presented in Figure 9.

Table **1** – XRMC results for samples 24_42 and 24_43.

Spot	N. Inv.	Cu	Sn	Pb	Fe	Zn	As	Others	Patina thick.	Impurities
1	24_42	73.40	17.20	3.90	1.00	0.20	2.70	1.60	27 µm	Ag, Ni. Sb
2		79.65	13.30	2.90	0.60	0.20	2.30	1.05	38 µm	Ag, Ti. Ni, Sb
3		83.10	9.30	4.10	0.50	0.20	2.10	0.70	34 µm	Ag, Ni, Sb
4		73.55	19.95	3.30	0.25	0.20	1.85	0.90	24 µm	Ag, Bi, Ni, Sb
1	24_43	71.85	18.00	5.95	2.50	0.20	1.50	-	32 µm	-
2		70.55	19.40	5.25	2.40	0.20	2.20	-	33 µm	-
3		82.10	9.20	5.20	1.80	0.20	1.50	-	31 µm	-

Apart from one spot in each sample that stands out from the rest (spot 3 of each dagger), the results obtained are rather concise. Both daggers present a similar leaded bronze alloy with high tin content and a low percentage of arsenic, commonly occurring in copper ores and sometimes being inadvertently smelted together (Atzeni et al. 2005; Bottaini et al. 2017).

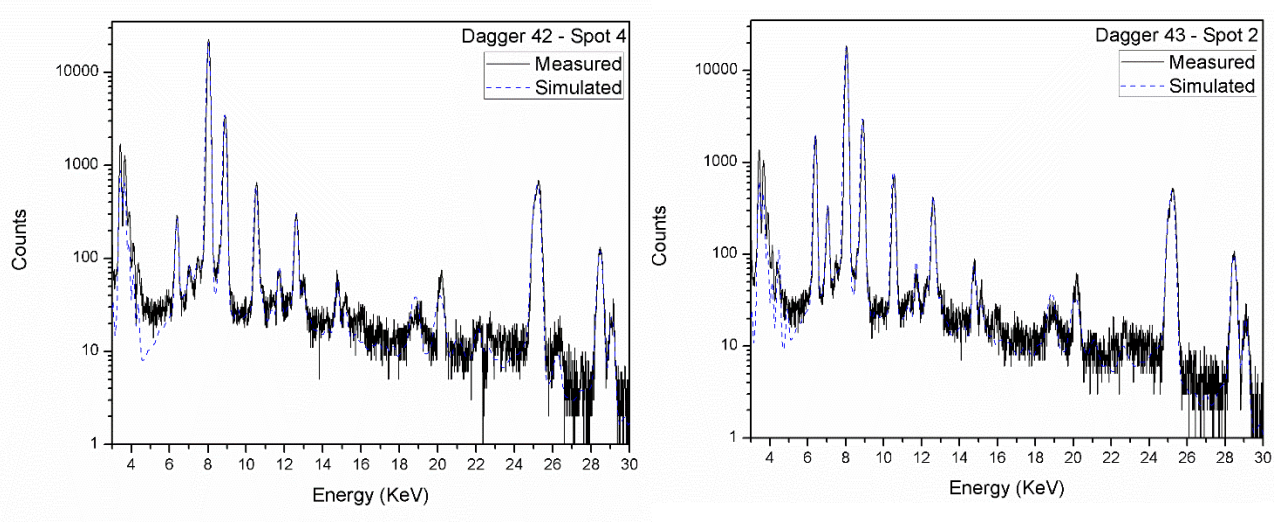

Figure **9** – Comparison between simulated and measured spectra of spots 4 and 2 for samples 24_42 (left) and 24_43 (right), respectively.

The discrepancy observed in tin content within the afore-mentioned spots may result from accidentally picking a spot where Cu-Sn segregation occurred in a high degree. With such

high quantities of tin, a segregation occurs more easily, originating in the formation of tin-rich and copper-rich phases (Callister 2007).

The low amounts of zinc and iron does not come as a surprise. Iron is rather common in such low percentages and can come from both the ore used and from the flux added during the smelting process (Craddock 1976; Ingo et al. 2006). This particular element can be also used as a sign of technological level and skill of the metalworker, where low amounts (around 0.3 wt%) are signs of a more efficient smelting process (Ingo et al. 2006).

Iron, in raging concentrations has been reported in some *navicelle* and other nuragic objects (Brunetti et al. 2015; A. Brunetti, Depalmas, et al. 2016; Schiavon et al. 2013, 2016) and in lower concentrations – averaging 0.35 wt% – to be consistent with EIA bronzes from whole Mediterranean (Schiavon et al. 2013).

Zinc, as arsenic, occurs frequently in Sardinian mineralization and is reported in some authentic objects such as the *Maracalagonis* sword (Atzeni et al. 2005), a bronze bun-ingot from *Sant'Anastasia di Sardara* (Moravetti et al. 2014), some *bronzetti* preserved at Musei di Providence, Detroit (Lilliu 2008) and as trace element – in the order of ppm's – within several other daggers (Atzeni et al. 2005). Curiously, another object from *Sardara*, namely an archer figure (*bronzetto*), presents 1 wt% Fe content (Schiavon et al. 2013), compatible with dagger 42 composition.

The impurities found within Dagger 42 can attest in favor of its originality. Antimony and bismuth are observed in couple other nuragic objects and copper ingots, also suggesting the extraction of copper from minerals such as covellite, tennantite, enargite and chalcocite (Atzeni et al. 2005) or the use of such ingots for casting the object. Silver is also reported as present in some other objects, and found in quantities between 0.05 and 0.25 wt% in 5 bronze objects from *Monte Baranta* (one spatula and 4 tanged daggers) (Atzeni et al. 2005).

Titanium, which is usually attributed to soil incrustations, is here associated to the bulk of the material probably due to limitations of the MC protocol and to the complex samples' structure, having sometimes a transition layer between the bulk of the material and the outer corrosion layer and being difficult to simulate with precision.

Nickel is usually present in native copper together with selenium, arsenic, antimony, gold and silver in small proportions and is reported as trace element in 32 copper ingots fragments from *Baccus Simeone*, *Villanovaferru* and other copper fragments from *Baradilli* (Atzeni et al. 2005).

Whereas the corrosion is concerned, sulfur and chlorine are present in every analyzed spot from Dagger 42. Iron is found in varying concentrations ranging from 0.25 to 2.20 wt% and titanium is found except in spot 4 and between 0.20 and 0.35 wt%. The patina thickness observed is compatible with Robbiola's type I corrosion (Robbiola et al. 1998), typical of quaternary bronzes.

Dagger 43 presents a coherent chemical composition, also compatible with most of the reported findings in this section, presenting only a larger amount of iron and tin. Its corrosion layer presents a very similar composition to Dagger 42, containing sulfur, chlorine and titanium in similar amounts but overall higher tin content. Iron content varies from 2.2 to 2.8 wt%.

The detected impurities in Dagger 42 suggests the use of native copper.

- *Dagger 44*

This particular dagger is curious because of its shape and size, having few parallels in literature. Nevertheless, Dagger 44 can be confronted with two other somewhat similar daggers listed in Minoja et al. and Moravetti et al., namely objects number 816 (p. 816) and 31 (p. 316) respectively. (Minoja et al. 2015; Moravetti et al. 2014).

The analyzed spots were only two for this object. The results obtained with the MC protocol are listed in Table 2 below.

Table **2** – XRMC results for sample 24_44.

Spot	N. Inv.	Cu	Sn	Pb	Fe	Zn	As	Others	Patina thick.	Impurities
1	24_44	71.20	18.20	9.10	0.20	-	1.20	0.10	26 μm	Ni
2		69.30	20.20	9.20	0.20	-	1.00	0.10	34 μm	Ni

The sample was simulated as a 2-layered structure in the same way as daggers 42 and 43, presenting a corrosion layer of 26 and 34 μm (for spots 1 and 2, respectively) and the bulk material, composed of a high tin leaded bronze alloy.

Both spots analyzed are consistent between themselves concerning chemical composition. Tin content is extremely high, being very unusual for objects related to the nuragic civilization and hardly reported in literature as overpassing a threshold of around 15 wt%. Nevertheless, Robbiola et al. (Robbiola et al. 1998) reported the chemical composition of a Cu-Sn alloy axe (between other objects) from western France Bronze Age containing 22 wt% Sn and an ingot containing 18.2 wt% Sn.

Iron and arsenic concentrations are compatible with ancient bronzes taking into account the ores used for smelting of copper in ancient times, already discussed in this section. Their contents show parallels with several other daggers and artefacts from nuragic times and iron content compatible with most of EIA Mediterranean bronze objects (Schiavon et al. 2013).

Lead in the presented amount is usually found within nuragic bronzes from Iron Age (900-600 BC) (Schiavon et al. 2016), but not together with the corresponding tin quantity.

The corrosion layer presents similar amounts of tin and copper, suggesting a high quantity of tin corrosion products, estimated around 12 wt%. Moreover, several signs of incrustation were detected, such as the presence of calcium, potassium and silicon within the corroded layer. Titanium and iron are also detected in 0.20 and 0.80 wt% respectively.

Again, the patina thickness observed is consistent with Robbiola's type I corrosion, characteristic of quaternary bronzes (Robbiola et al. 1998).

Typical corrosion-related elements as sulfur and chlorine were also detected but in lesser amounts than those reported in Daggers 42 and 43. This may be due to the proportion between tin and copper corrosion products being higher than usual. Obviously, for a more throughout and precise evaluation of the corrosion products, other analytical techniques are better advised.

The excessive amount of tin comes as a surprise, but the reasons for it can be manifold. Either the ancient metalworkers added more tin than usual to this object in the attempt of further improving mechanical properties (since the addition of tin is already known at the time to improve this feature) or the analyzed spots were poorly selected, representing a composition of tin-rich phases instead of the real average composition of the object. Another hypothesis is the unadvised use of bronze ingots with tin ingots instead of copper ingots + tin ingots, resulting in a high-tin bronze-alloyed object.

In the other hand, tin was as a very precious and expensive metal for the nuragic people during the Bronze Age, not readily available in Sardinia and being obtained through several exchange routes throughout the Mediterranean. Therefore, the reasons to add such an excessive amount to an object are not coherent with the reality of the time.

Meeks (Meeks 1993) report the existence of high tin bronzes (19 – 27% Sn) in the past, but in a context where a silvery and shining surface was desired. The Romans, for instance, made use of leaded high tin bronzes to manufacture mirrors.

It is hard to attest that this particular dagger is indeed a nuragic production. The use of a leaded high tin alloy, with low arsenic concentration is uncommon to the nuragic civilization. The dagger may have been the product of re-melting and re-use through time or imported.

- *Bronzetto 47*

The *bronzetti* are the most known and widespread manifestation of the nuragic culture, representing a series of activities and features intrinsic to the nuragic culture itself and commonly found in a votive/ritualistic/religious context (Melis 2003; Webster 2014). There are several hundreds of *bronzetti* catalogued nowadays and preserved in museums worldwide. This particular object, the *Bronzetto* n. 47, is a classical representation of an archer and appears heavily corroded. Parallels can be drawn with some archer *bronzetti* depicted in Lilliu's catalogue and Moravetti et al. work (Lilliu 2008; Moravetti et al. 2014).

For the application of the MC protocol, three spots were analyzed. Spots 1 and 2 were taken in the vicinity of each other, spot 1 presenting clear visual signs of oxidation. The results obtained are listed in Table 3 below.

Table **3** – XRMC results for sample 24_47.

Spot	N. Inv.	Cu	Sn	Pb	Fe	Zn	As	Others	Patina thick.	Impurities
1		74.30	15.30	6.90	0.45	0.20	2.85	-	25 μm	-
2	24_47	70.50	17.10	8.10	1.35	0.20	2.75	-	33 μm	-
3		74.00	15.10	8.10	0.70	0.20	1.90	-	31 μm	-

It is easy to observe that this *bronzetto* is made of a leaded bronze alloy with high tin content. The low amount of zinc and iron, in a similar way to that of Daggers 42 and 43, is characteristic of Sardinian mineralization (Atzeni et al. 2005) and suggests the usage of metals from native ores. Nevertheless, the corrosion thickness presented is more compatible to quaternary bronzes than leaded, arsenical or typical tinned bronzes (Robbiola et al. 1998).

Lead, in the ranging concentrations, is compatible with several nuragic objects already mentioned in the above discussions. The same observation is valid for arsenic content. Nevertheless, concerning *bronzetti* statues, the average lead content is usually smaller (less than 1 wt%). Chemical analysis of a set of 12 *bronzetti* from the National Archaeological Museum in Cagliari (Sardinia, Italy) – presented at Atzeni et al. work – reports lead concentrations between 0.06 and 0.99 wt%, and only one *bronzetto* to have a concentration

of 6.50 wt% Pb. Tin content varies from 5.9 to 13.1 wt%. No arsenic is reported to be present in this set of *bronzetti*. It is important to mention that this set of objects is from a same location, with only one third being from unknown locations.

A set of 31 fake *bronzetti* were chemically analyzed and the results are reported at Atzeni et al (Atzeni et al. 2005). The chemical composition varies significantly as expected, presenting zinc concentrations ranging from 0.1 to 10.8 wt%, with an average value of 3.90 wt% and a standard deviation of 2.68. Tin content averages 5.56 wt% with a maximum of 13.20 wt% and lead content averages 4.10 wt% with a maximum of 10.30 wt%. The iron content reported in the fakes is consistent and averaging 0.45 wt%.

The three fakes presenting the lowest zinc contents of 0.1, 0.2 and 0.4 wt%, therefore somehow similar to *Bronzetto* 47, contain 4.1, 3.3 and 4.4 wt% Sn and varying contents of lead; 6.5, 3.4 and 1.5 wt% respectively. No arsenic is reported in any of the analyzed fakes. It is safe to infer that this particular *bronzetto* does not fit within the average chemical composition presented by a large group of fakes.

Concentrations of copper and tin within the corrosion layer are found to be in similar amounts for every analyzed spot, averaging 11 wt% each. Soil incrustation is possible to be present since the existence of silicon, phosphorous, potassium and calcium within the corroded layer is reported. Again, elements associated to copper corrosion products such as sulfur and chlorine are also reported. Iron and titanium were detected in the corrosion layer. Iron, averaging 0.55 wt% and titanium, 0.14 wt%.

Despite spots 1 and 2 being selected close to each other, and spot 1 presenting a clear oxidized surface, the differences are minimal and restrain to a lower lead content in spot 1 and to an absence of incrustation signs in spot 2. Moreover, spot 3 – presenting no clear sign of oxidation – is shown to present a corrosion composition closer to spot 1 than spot 2. For further understanding, more investigation is required, and with the data gathered solely by the XRMC protocol nothing beyond speculation can be discussed in this regard.

- *Navicella 24_49*

A total of three spots were analyzed by means of XRF for the application of the MC protocol. Two spots were selected in the left side of the ship and one at the bottom. The two lateral spots were chosen as follows: one in a "clean" spot (spot 1) and another over a clear sign of encrustation (or oxidation) (spot 2). A micrograph of the spots taken with the ELIO spectrometer camera in shown in Figure 10. This choice yielded a significant and expected difference in results. Spot 2 presented significantly less iron content than spot 1, arsenic (0.10 wt%) and 2 wt% more tin than spots 1 and 3. Chromium was found to be present only in spots 1 and 3 at 0.60 wt% and 0.80 wt%, respectively. Spot 2 also presented considerable more zinc content than the other analyzed spots (Table 4) and a higher content of copper in the corrosion layer (21 wt%).

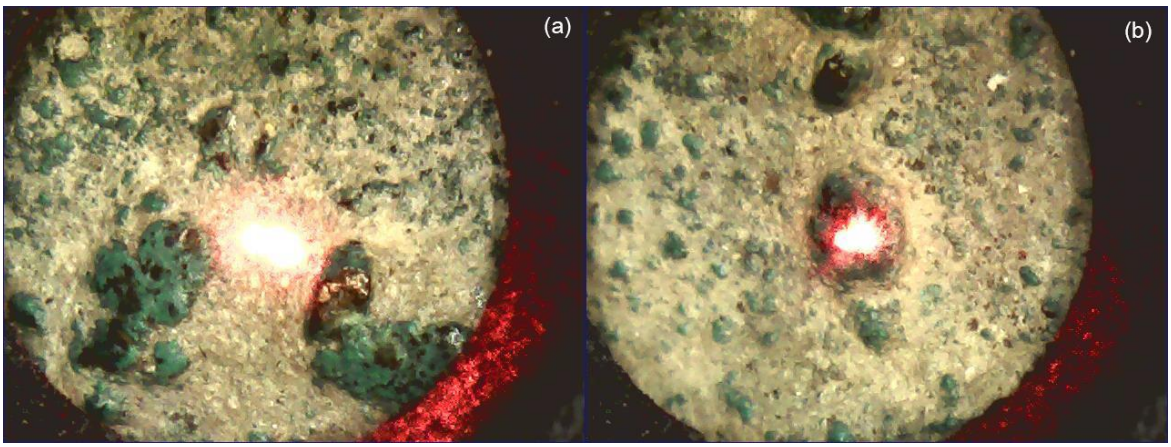

Figure **10** – Micrograph of sample 24_49 spots 1 (a) and 2 (b).

Spot 2 is off-consideration for representing an accurate description of the samples' true composition since it differs deeply from the other analyzed spots. Therefore, spots 1 and 3, presenting a similar elemental composition, points that the *Navicella* boat is made of a quaternary copper alloy (Cu-Sn-Zn-Pb) containing approximately 77 wt% Cu and a superimposed corrosion layer of around 100 μm in thickness. The superimposed layer contains around 10 wt% Cu and small amounts (less than 2 wt%) of S, Cl, K, Mn and Ni. Sulfur and chlorine are common in copper corrosion products such as atacamites, nantokite, chalcocite and covellite. The other elements can be derived from soil incrustations.

Table **4** – XRMC results for sample 24_49.

Spot	N. Inv.	Cu	Sn	Pb	Fe	Zn	As	Others	Patina thick.	Impurities
1		71.40	3.40	9.00	9.60	6.00	-	0.60	98 µm	Cr
2	24_49	73.85	5.50	10.15	1.30	9.10	0.10	-	96 µm	-
3		83.10	3.40	4.50	3.20	5.00	-	0.80	110 µm	Cr

A difference in lead and iron contents between spots 1 and 3, namely 9.0 wt% and 9.6 wt% for the former and 4.5 wt% and 3.2 wt% for the latter, respectively, suggests that the object was casted upside-down. Heavier elements tends to migrate by gravity during the casting process resulting in a Cu-Pb segregation. This is due not only to a gravity gradient, but also to the inherent low-miscibility between the two metals (Quaranta et al. 2014).

Zinc is reported to be found in some Cypriot bronzes from 11th to 8th centuries BC, but in percentages never exceeding 1 wt%, suggesting that their use was not intentional (Charalambous et al. 2014). Moreover, zinc sulphides are also associated to Montevecchio's galena (de Caro 2017), but again, the zinc concentration present in the final object would very unlikely reach high percentages such as the ones reported in the analyzed *Navicella*.

Concerning the originality of the artefact, although it matches the typology of some nuragic *navicelle* described in Lilliu's catalogue (Lilliu 2008), it is clear from the chemical composition that this *navicella* is a later reproduction of an original nuragic votive ship. Zinc was very unlikely to be used as an intentional alloying element during the nuragic Bronze Age or Iron Age and high contents of this metal is usually a sign of falsification (Atzeni et al. 2005). Moreover, the excessive amounts of zinc are also compatible with that if several fake bonze figurines listed in Atzeni et al. works' Chapter 1, section L (Atzeni et al. 2005).

- *Bronzetto 52*

This particular object is similar to many other *bronzetti* in dimensions and depicts an anthropomorphic figure with the left arm uplifted. The right arm and head of this *bronzetto* are missing and a clear later addition of a metallic rod to the left foot is observed. This rod is inserted onto a wooden pedestal to hold the figure standing. The object was analyzed in three distinct spots and the results obtained with the MC protocol are listed in Table 5 below.

Table **5** – XRCM results for sample 24_52.

Spot	N. Inv.	Cu	Sn	Pb	Fe	Zn	As	Others	Patina thick.	Impurities
1		81.30	13.05	0.70	0.10	0.55	4.30	-	89 µm	-
2	24_52	89.45	3.40	0.90	0.60	-	5.15	0.50	120 µm	Cr
3		89.85	3.40	0.90	0.20	-	5.15	0.50	92 µm	Cr

Differently from *Bronzetto* 47, the XRMC data, at first, suggests that this particular *bronzetto* is made of an arsenical bronze. It is evident that tin content between spot 1 and the others is entirely different. The reason for this may be the same as for Daggers 42 and 43. Nevertheless, the segregation that occurs between tin and copper is more pronounced at high tin quantities (Callister 2007; Selwyn 2004), being somewhat incompatible with low percentages of tin rounding 3 wt%. The casting method (usually lost-wax for the production of *bronzetti* – (Moravetti et al. 2014)) is unlikely to be the cause for the observed phenomenon, since spots 1 and 3 are in different heights of the object and spot 2 is in the mid-point (Annex A). Sometimes the casting method can interfere in the homogeneity of the composition, creating a gradient throughout the object.

Figure 11, below, shows a comparison between the measured and simulated spectra for spots 1 and 2. The mismatched peaks between 18 and 22 KeV are Compton peaks.

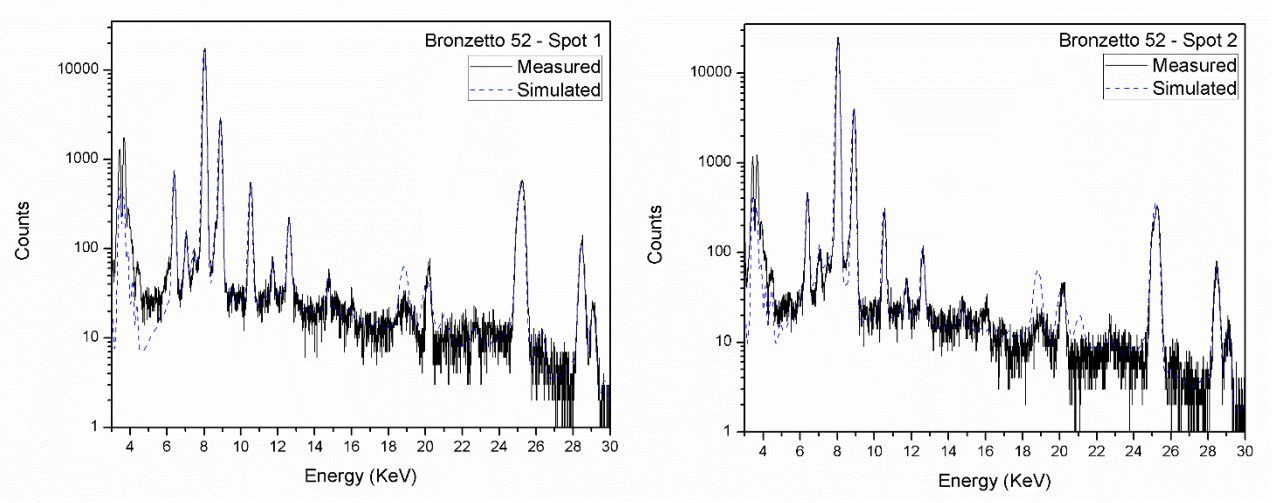

Figure **11** – Comparison between simulated and measured spectra of spots 1 (left) and 2 (right) for sample 24_52.

Chromium content rounding up to 0.50 wt% within archaeological samples from the Sardinian Bronze Age or Iron Age is hardly reported in literature. One of the few mentions of chromium in an archaeological perspective is found in Stos-Gale et al. work. According to them, sulphides mineralization from Limassol Forest, Cyprus (about 20 Km from Kalavasos) contains chromium in quantities averaging 0.39% with a maximum of 4.76%. These sulphides also contain arsenic, and could be very well used as a convenient source of raw material for producing arsenical copper in Early and Middle Cypriot periods (Stos-Gale et al. 1997).

Nevertheless, Stos-Gale et al. also observe that prior to the exploitation of Limassol Forest mineralization in the 1950's, there was no sign of ancient workings and all veins were intact up to the surface, pointing out towards a strong evidence that no ancient exploitation took place.

It is easier to assume that chromium is present as an impurity or contamination from soil or storage conditions rather from present in the original metal used for manufacturing the artefact. All analyzed objects in this work come from a private collection. Therefore, it is hard to know in which exact conditions the objects were stored during their "after-

excavation" life. One hypothesis may be the contamination by wood, since chromated copper arsenate (CAA) is by far the most popular wood preservative being introduced in the 1940's (Barnhart 1997; Hingston et al. 2001).With a favorable environment (pH and humidity) CAA-treated wood could contaminate the objects' surface upon long periods of storage.

The patina thickness determined by the MC protocol is compatible with Robbiola's type II corrosion, more specifically within the range of tinned bronzes – between 40 and 138 μm. Type II corrosion is coarse and the original surface of the object is usually undistinguishable. In this case, it appears that the corrosion layer is more of a type I corrosion, but thicker.

Spot 1 presented a lighter corrosion layer than the other two and minor amounts of zinc and nickel, 0.10 and 0.03 wt% respectively. Copper content within the layer was similar to that of tin and around 10 wt%, while spots 2 and 3 presented over 25 wt% Cu. The latter two also presented 0.10 wt% Ti. Sulfur and chlorine were present in higher quantities as well.

Tying up the data, it is clear that spot 1 is different from the other two in every aspect. The higher content of tin, together with a lighter and somewhat thinner corrosion layer may be interpreted as a sign of lesser corrosion and therefore less tin depletion occurred when in comparison with spots 2 and 3. The thickness of the patina limits the penetrating effects of the X-ray beams, hindering a precise acquisition of bulk data and yielding a composition value corresponding to a region closer to the border between the corrosion layer and the objects' original surface.

Another effect that can be caused by corrosion in high-tin bronzes is the formation of a tin-rich layer just above the "inner" corrosion layer (Nørgaard 2017; Robbiola et al. 1998). If this is the case, spot 1 presents misleading information, reflecting a composition and structure not close enough to the real one. Therefore, more simulations are still required, creating a 3-layered structure composed of substrate, inner corrosion layer and tin-rich outer corrosion layer.

The data presented for this particular object is inconclusive and further analysis is required.

- *Double axe 110*

This axe shares common features with few other unearthed axes tied to the nuragic culture and civilization. Double-axes, more specifically "*axe-adze"* or *"maleppeggio"*, possessing two cutting edges orthogonal to each other, are not original from Sardinia and are said to be a Cypriot model either imported or imitated by Sardinians (Atzeni et al. 2005). Matrices used for the crafting of this specific type of axe are reported in literature (Atzeni et al. 2005; Moravetti et al. 2014) and found within few nuragic sites in Sardinia Island.

Four spots were chosen for evaluating this object and for the validation of the MC protocol: two within the flat edge (parallel to the handle), one at the handle insert and a last one at the orthogonal cutting edge (further information is shown in Annex A).

The results obtained with the MC protocol are listed in Table 6 below.

Table **6** – XRMC results for sample 110.

Spot	N. Inv.	Cu	Sn	Pb	Fe	Zn	As	Others	Patina thick.	Impurities
1	110	82.65	7.90	4.80	0.25	-	4.40	-	82 μm	-
2		87.70	5.10	3.00	0.10	-	4.10	-	94 μm	-
3		85.87	6.60	4.10	0.33	-	3.10	-	82 μm	-
4		78.40	11.10	5.50	0.60	-	4.40	-	72 μm	-

The results observed are consistent and all spots share similar characteristics, except for spot 4, richer in tin content and presenting a thinner corrosion layer. Despite presenting a thinner corrosion layer, spot 4 also presented high quantities of calcium, potassium and silicon – typically interpreted as signs of soil contamination/incrustation. Spot 2, presenting

the lower percentage of tin, has a Cu-rich corrosion layer. A comparison between spots 3 and 4 measured and simulated spectra is shown in Figure 12.

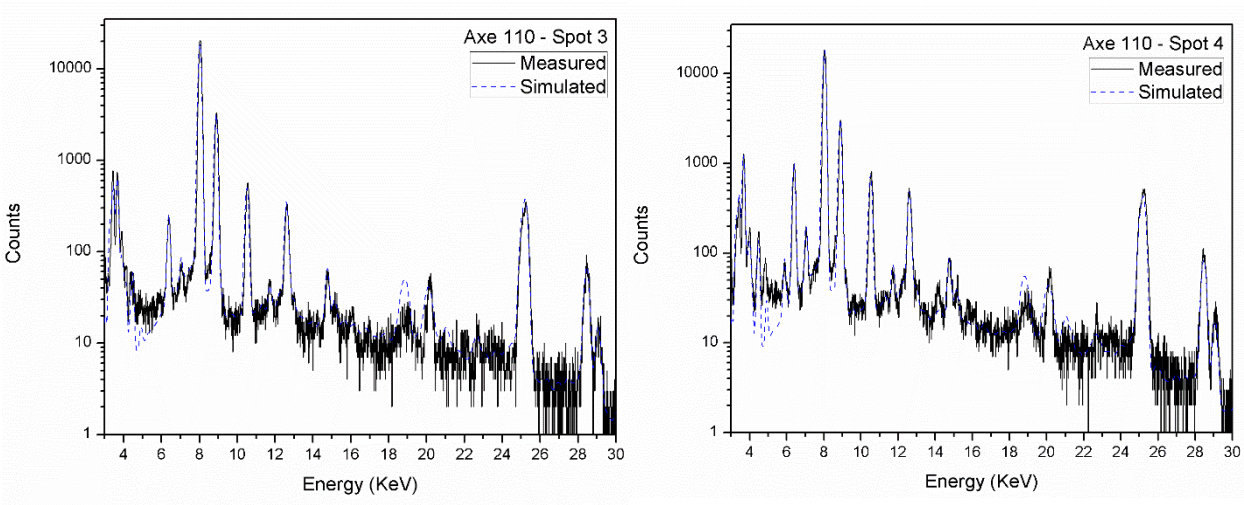

Figure **12** – Comparison between simulated and measured spectra of spots 3 (left) and 4 (right) for sample 110.

Titanium is again found within the corrosion layer of every analyzed spot and in concentrations averaging 0.50 wt%. Manganese is detected in spot 4 (0.10 wt%) together with iron (1.20 wt%).

Spot 4 may contain misleading information. The reasons may be those presented earlier for *Bronzetto* 52, spot 1. The simulated structure (a 2-layered structure) does not accurately represent the real one, not taking into account the possible formation of another (inner) tin-rich layer. The miss-simulation, in this case, produced a thinner corrosion layer and a higher tin content within the bulk of the sample, whereas a better and more accurate simulation would yield a thicker total corrosion surface and a lower tin content for the bulk.

It is worth mentioning that the miss-simulation of one particular spot does not invalidate the others, mostly for the presented case. Corrosions of type I and II are not exclusive and may be found within the same object in different parts. Therefore, the existence of a tin-rich layer may be only noticed in a particular part or spot of the object, while absent in others (Robbiola et al. 1998). Figure 13 below shows the surface where spot 3 was measured.

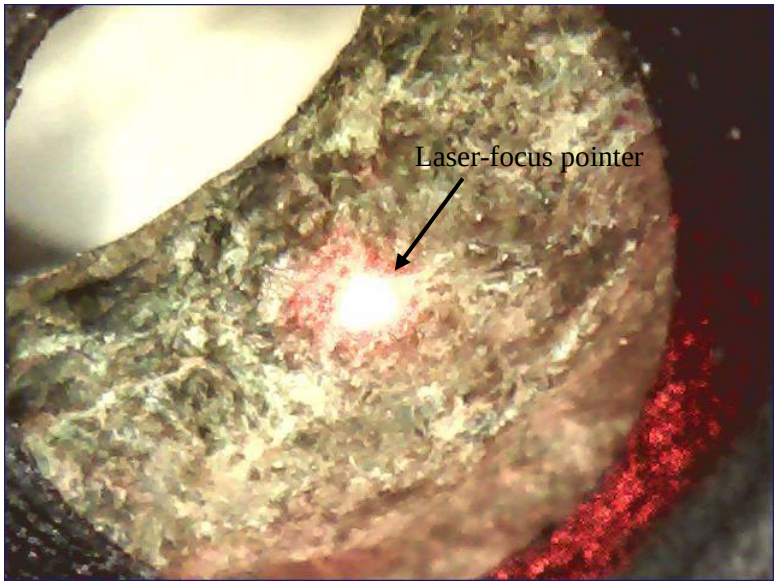

Figure **13** – Micrograph of sample 110 surface (spot 3).

Nevertheless, the remaining spots, namely 1, 2 and 3, can be still interpreted as a good representation of the real structure and composition of the object. The lower iron content and the leaded bronze alloy employed, containing a considerable amount of arsenic, are compatible with Mediterranean Bronze Age. The iron content attests a skillful casting and smelting ability of the metalworker.

Arsenical copper was widespread in the Early and Middle Cypriot Bronze Ages, being only replaced by bronze in a later period. The appearance of arsenical bronzes is likely to have been a result of mixing imported bronzes with local Cu-As alloys. The use of tin-bronzes was first limited to specific objects, as riveted knives, while scrapers, tweezers, hook tang weapons and pins were made of arsenical bronze. It was only during the Late Bronze Age that tin-bronzes were finally stablished as a standard alloy (Atzeni et al. 2005).

This particular axe may have been the result of a local Sardinian re-melting, using leaded-bronze and arsenical bronze (or arsenical copper) or an import from Cyprus, where this type of axe was more common.

- *Axe 111*

This is a rather common axe with a considerable amount of parallels from nuragic Sardinia. It presents a simple profiled shape with one flat cutting edge. Some molds for casting this type of axe are also reported in literature (Atzeni et al. 2005; Moravetti et al. 2014). The mold required for the casting of such an axe is likely to be composed of two or more stones, due to the dimensions and shape of the object. Simple flat axes are cast in a single stone molds (Atzeni et al. 2005).

The results obtained with the MC protocol are listed in Table 7 below.

Table **7** – XRMC results for sample 111.

Spot	N. Inv.	Cu	Sn	Pb	Fe	Zn	As	Others	Patina thick.	Impurities
1	111	79.10	7.40	3.40	10.10	-	-	-	60 μm	-
2		76.65	13.90	2.85	5.40	-	0.15	1.05	62 μm	Ti + Cr
3		84.30	10.40	1.50	3.80	-	-	-	67 μm	-
4		77.80	14.00	3.80	3.20	-	1.20	-	62 μm	-

Axe 111 presents different compositional values from every other analyzed object so far. The relative high amount of iron is unexpected and uncommon regarding authentic bronze objects from Mediterranean Bronze Age. Iron in ancient times was an extremely good quality material and hard to manipulate, requiring advanced forges capable of reaching higher temperatures.

Low amounts of iron, around 1 wt%, are acceptable for bronze objects dating from the Mediterranean Bronze Age. Its unadvised addition to the alloy would come as a result from the ore smelting process. Higher amounts, as those found in the *Navicella* 49 and in this particular axe are, at least, atypical.

Adding further, the miscibility between iron and copper is relatively low (Lukyanov et al. 2014) and their combined use for creating usable alloys requires a great deal of technology even nowadays. Therefore, their combined use in ancient times for casting weapons or tools (assuming it was possible) would yield extremely fragile objects, hindering their use.

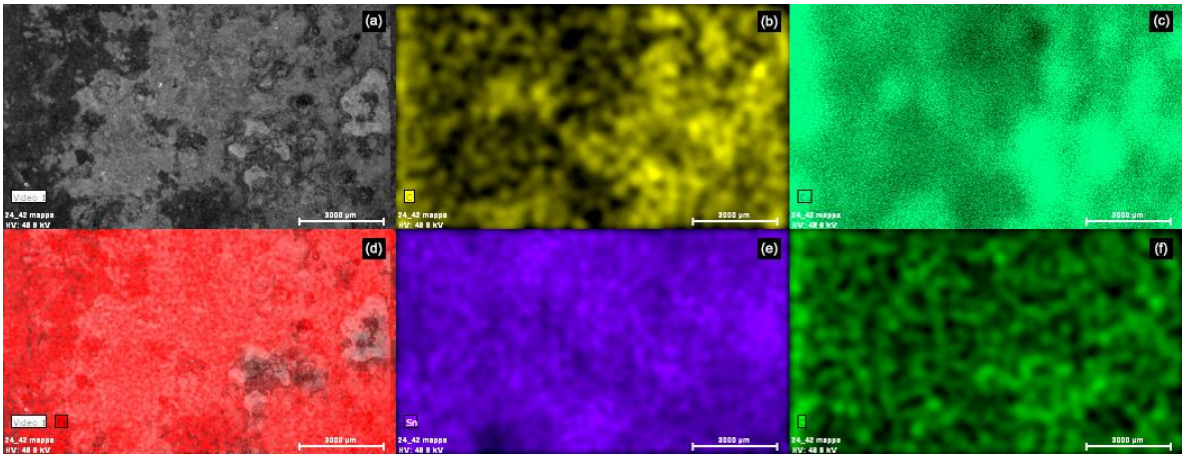

Figure **14** – Elemental map distribution of sample 111 surface optical image (a), elemental distribution of Cl (b), Cu (c), Fe (d), Sn (e) and O (f).

Patina thickness seems homogeneous within the whole object, but its composition is clearly heterogeneous as presented in Figure 14 above. The darker areas (Figure 14a and Figure 14d) evidence the higher concentration of iron. The lighter areas on the right portion of the micrograph (Figure 14a and Figure 14c) are attributed to copper corrosion products, mostly chlorides, as suggested by Figure 14b. Tin is spread throughout the objects' surface, and shows no correlation with copper-rich or iron-rich areas.

The XRMC protocol displayed a very low tin and copper content within the corrosion layer. Spot 4 is almost void of tin, presenting only 0.50 wt%. Copper content averages 15 wt%, except for spot 2, where it is only present at 4.6 wt%. Iron is presented in relatively high quantities, between 2.20 and 5.00 wt%.

The reasons for such an atypical chemical composition, low copper content within patina and for the relatively high amount of iron cannot be discussed beyond speculation. This

object may not be an authentic production due to its corrosion features and unusual iron content within the bronze alloy.

- *Boat head 114*

Zoomorphic figures attached to or cast as a single piece together with boat figurines (*navicelle*) are a rather common manifestation of the nuragic culture. The species depicted varies and are discussed elsewhere (Lilliu 2008; Moravetti et al. 2014).

For this object, only two spots were selected for analysis and the results obtained are presented in Table 8 below.

Table **8** – XRMC results for sample 114.

Spot	N. Inv.	Cu	Sn	Pb	Fe	Zn	As	Others	Patina thick.	Impurities
1	114	38.70	9.10	50.00	1.20	-	1.00	-	38 μm	-
2		33.00	10.50	54.00	1.00	-	1.50	-	62 μm	-

The MC protocol yielded a compositional value that suggests the mixing of copper (or bronze) with lead to create the alloy. Lead working in Sardinia dates back to the Chalcolithic period (~2400 BC) and a large amount of lead objects are related to the nuragic period, being a common occurrence (Atzeni et al. 1991).

Little information is given concerning the compositional values of lead objects from the nuragic period. Some are listed in Atzeni et al. work (Atzeni et al. 2005) and the objects evaluated are reported to be made almost entirely of lead. Moreover, lead ingots, scraps, cramps for repairing pottery and other objects were recovered from nuragic sites and, as before said, are taken to be a common occurrence.

The mixing of copper, tin and lead is discussed in literature (Atzeni et al. 1991, 2005) but in a perspective where small amounts of lead are considered and taking into account the

casting of leaded bronze alloys. A mixture of roughly five parts of lead to four parts of copper within this context – to the authors' knowledge – is so far unreported in literature.

Nevertheless, it is not unlikely that ancient metalworkers would mix a considerable amount of lead to bronze for casting new objects. Lead was readily available in the island and abundant. This combined use with bronze may have been an attempt of the metalworker to cast an object in a "cheaper" way, still maintaining the color and some characteristics of typical bronzes. Mechanical properties can be considered irrelevant (to a certain extent) when dealing with votive or decorative objects, so the excessive amount of lead would not affect the "usability" of the object.

Patina thickness varies greatly between both analyzed spots and presents a rather "light" composition, with low amounts of tin, copper and lead (ranging from 1 to 5 wt%). Iron is found in minor quantities (0.20 wt%). Calcium and potassium are detected in small amounts in the average of 1.0 wt% and chlorine and sulfur, characteristic of copper corrosion products, in amounts around 3 wt%.

7 Conclusions

The following conclusions can be drawn from the experimentation conducted:

- The Monte Carlo protocol proved to be a powerful tool in determining the composition and structure of most archaeological objects studied;
- In some specific cases, as present in the discussion of objects 110 and 24_52, the protocol adopted still require further enhancements and tweaks so a more accurate simulation of the structure and composition can be achieved;
- Attesting the authenticity of ancient objects solely by the use of XRF combined with MC protocol is a challenging task. When the chemical composition is not obviously different (in the mean that it is immediately seen that the alloy is not compatible with ancient metalworking products) it hard to attest with certainty the originality of the object;
- Some objects are possibly original metalworking products of an ancient civilization and in addition, compatible with the Mediterranean Bronze Age. These objects are: Dagger 42, 43, *Bronzetto* 47 and the Double-axe 110;
- The results obtained from *Bronzetto* 52 are somewhat inconclusive and further analysis are still required;
- *Navicella* 49 is possibly a fake production and Axe 111 may be a fake production as well, although it cannot be said with certainty for the latter;
- A succinct resolution of an average composition and corrosion features of ancient bronzes from the Mediterranean basin was successfully established.

REFERENCES

Alonso, Ma P. et al. 2009. “Caracterización de Un Vidrio Rojo Medieval Procedente de Las Vidrieras Del Monasterio de Las Huelgas de Burgos.” *Boletin de La Sociedad Espanola de Ceramica y Vidrio* 48(4):179–86.

Angelini, E. et al. 2014. “The Role of Surface Analysis in the Strategies for Conservation of Metallic Artefacts from the Mediterranean Basin.” *Surface and Interface Analysis* 46(10–11):754–63.

Attanasio, D., G. Bultrini, and G. M. Ingo. 2001. “The Possibility of Provenancing A Series of Bronze Punic Coins Found At Tharros (Western Sardinia) Using the Literature Lead Isotope Database.” *Archaeometry* 43(4):529–47. Retrieved (http://doi.wiley.com/10.1111/1475-4754.00035).

Atzeni, C., L. Massidda, U. Sanna, and P. Virdis. 1991. “Notes on Lead Metallurgy in Sardinia during the Nuragic Period.” *Historical Metallurgy (Journal of the Historical Metallurgy Society)* 24(2):97–105.

Atzeni, Cirillo et al. 2005. *Archaeometallurgy in Sardinia: From the Origins to the Beginning of the Early Iron Age*. edited by F. Lo Schiavo, A. Giumlia-Mair, U. Sanna, and R. G. Valera. Montagnac: Éditions Monique Mergoil.

Balmuth, M. S. and RF Tylecote. 1976. “Ancient Copper and Bronze in Sardinia: Excavation and Analysis.” *Journal of Field Archaeology* 3(2):195–201. Retrieved (http://www.jstor.org/stable/529386).

Barcellos Lins, Sergio Augusto, José Humberto Zani, and Joaquim Teixeira De Assis. 2015. “Caracterização de Fósforos de lâMpadas Fluorescentes Através de Espectroscopia Por Fluorescência de Raios-X.” in *I Encontro de Engenharia, ciência de materiais e inovação do Estado do Rio de Janeiro*. Nova Friburgo.

Barnhart, Joel. 1997. “Occurrences, Uses, and Properties of Chromium.” *Regulatory Toxicology and Pharmacology* 26(1):S3–7. Retrieved August 22, 2018 (https://www.sciencedirect.com/science/article/pii/S0273230097911326).

Becker, Marshall Joseph. 1980. “Sardinia and the Mediterranean Copper Trade: Political Development and Colonialism in the Bronze Age.” *Anthropology* 4(2):91–117.

Beckhoff, Burkhard, Helmut Wolff, Norbert Langhoff, Reiner Wedell, and habil. Birgit Kanngießer. 2006. *Handbook of Practical X-Ray Fluorescence Analysis*. 1st ed. edited by B. Beckhoff, B. Kanngießer, N. Langhoff, R. Wedell, and H. Wolff. Springer Berlin Heidelberg. Retrieved (http://dx.doi.org/10.1007/978-3-540-36722-2%5Cnhttp://www.springerlink.com/content/q843r6/?p=db30d698476e45c9aa5fdca5e8620b6b&pi=0).

Begemann, Friedrich, Sigrid Schmitt-strecker, Ernst Pernicka, Lehrstuhl Archäometallurgie, and Fulvia Lo Schiavo. 2001. “Chemical Composition and Lead Isotopy of Copper and Bronze from Nuragic Sardinia.” *European Journal of Archaeology* 4(1):43–85.

Bernard, M. C. and S. Joiret. 2009. “Understanding Corrosion of Ancient Metals for the Conservation of Cultural Heritage.” *Electrochimica Acta* 54(22):5199–5205.

Bertolotti, Giulia et al. 2012. “Micro-Raman Study of Copper Hydroxychlorides and Other Corrosion Products of Bronze Samples Mimicking Archaeological Coins.” *Analytical and Bioanalytical Chemistry* 402(4):1451–57.

Bottaini, Carlo, Antonio Brunetti, Rui Bordalo, António Valera, and Nick Schiavon. 2017. “Non-Destructive Characterization of Archeological Cu-Based Artifacts from the Early Metallurgy of Southern Portugal.” *Archaeological and Anthropological Sciences* (May):1–10. Retrieved (http://link.springer.com/10.1007/s12520-017-0501-x).

Bottaini, Carlo Emanuele, Antonio Brunetti, Antonio Valera, and Antonio Candeias. 2018. “Use of Monte Carlo Simulation as a Tool for Non-Destructive ED-XRF Analysis of Archaeological Copper-Based Artifacts from the Chalcolitic Site of Perdigões, Southern Portugal.” *Applied Spectroscopy* 72(February):17–27.

Brunetti, A., A. Depalmas, F. Di Gennaro, A. Serges, and N. Schiavon. 2016. “X-Ray Fluorescence Spectroscopy and Monte Carlo Characterization of a Unique Nuragic

Artifact (Sardinia, Italy)." *Spectrochimica Acta - Part B Atomic Spectroscopy* 121:18–21. Retrieved (http://dx.doi.org/10.1016/j.sab.2016.04.007).

Brunetti, A., J. Fabian, C. La Torre, and N. Schiavon. 2016. "A Combined XRF/Monte Carlo Simulation Study of Multilayered Peruvian Metal Artifacts from the Tomb of the Priestess of Chornancap." *Applied Physics A: Materials Science and Processing* 122(6):1–8.

Brunetti, A., M. Sanchez Del Rio, B. Golosio, A. Simionovici, and A. Somogyi. 2004. "A Library for X-Ray-Matter Interaction Cross Sections for X-Ray Fluorescence Applications." *Spectrochimica Acta - Part B Atomic Spectroscopy* 59(10–11):1725–31.

Brunetti, Antonio and Bruno Golosio. 2014. "A New Monte Carlo Code for Simulation of the Effect of Irregular Surfaces on X-Ray Spectra." *Spectrochimica Acta - Part B Atomic Spectroscopy* 94–95:58–62.

Brunetti, Antonio, Bruno Golosio, Tom Schoonjans, and Piernicola Oliva. 2015. "Use of Monte Carlo Simulations for Cultural Heritage X-Ray Fluorescence Analysis." *Spectrochimica Acta - Part B Atomic Spectroscopy* 108:15–20. Retrieved (http://dx.doi.org/10.1016/j.sab.2015.03.014).

Buccolieri, Giovanni, Alessandro Buccolieri, Paola Donati, Maurizio Marabelli, and Alfredo Castellano. 2015. "Portable EDXRF Investigation of the Patinas on the Riace Bronzes." *Nuclear Instruments and Methods in Physics Research, Section B: Beam Interactions with Materials and Atoms* 343:101–9. Retrieved (http://dx.doi.org/10.1016/j.nimb.2014.11.064).

Callister, William D. Jr. 2007. *Materials Science and Engineering An Introduction*. 7th ed. John Wiley & Sons, Inc.

Di Carlo, G. et al. 2017. "Artificial Patina Formation onto Copper-Based Alloys: Chloride and Sulphate Induced Corrosion Processes." *Applied Surface Science* 421:120–27. Retrieved (http://dx.doi.org/10.1016/j.apsusc.2017.01.080).

Carmona, N., I. Ortega-Feliu, B. Gómez-Tubío, and M. A. Villegas. 2010. “Advantages and Disadvantages of PIXE/PIGE, XRF and EDX Spectrometries Applied to Archaeometric Characterisation of Glasses.” *Materials Characterization* 61(2):257–67.

de Caro, Tilde. 2017. “The Ancient Metallurgy in Sardinia (Italy) through a Study of Pyrometallurgical Materials Found in the Archaeological Sites of Tharros and Montevecchio (West Coast of Sardinia).” *Journal of Cultural Heritage* 28:65–74. Retrieved (http://dx.doi.org/10.1016/j.culher.2017.05.016).

Cesareo, Roberto. 2000. “X-Ray Physics: Interaction with Matter, Production, Detection.” *LA RIVISTA DEL NUOVO CIMENTO Della Scoietà Italiana Di Fisica* 23(7):1–231.

Cesareo, Roberto, Angel D. Bustamante, et al. 2013. “Multilayered Artifacts in the Pre-Columbian Metallurgy from the North of Peru.” *Applied Physics A: Materials Science and Processing* 113(4):889–903.

Cesareo, Roberto, Joaquim T. De Assis, et al. 2013. “Multilayered Samples Reconstructed by Measuring Kα/K β or Lα/Lβ X-Ray Intensity Ratios by EDXRF.” *Nuclear Instruments and Methods in Physics Research, Section B: Beam Interactions with Materials and Atoms* 312:15–22. Retrieved (http://dx.doi.org/10.1016/j.nimb.2013.06.019).

Cesareo, Roberto et al. 2015. “The Structure of Two-Layered Objects Reconstructed Using EDXRF-Analysis and Internal X-Ray Ratios.” *X-Ray Spectrometry* 44(4):233–38.

Cesareo, Roberto, Marcia A. Rizzutto, Antonio Brunetti, and Donepudi V. Rao. 2009. “Metal Location and Thickness in a Multilayered Sheet by Measuring Kα/Kβ, Lα/Lβ and Lα/Lγ X-Ray Ratios.” *Nuclear Instruments and Methods in Physics Research, Section B: Beam Interactions with Materials and Atoms* 267(17):2890–96. Retrieved (http://dx.doi.org/10.1016/j.nimb.2009.06.119).

Charalambous, Andreas. 2016. “A Diachronic Study of Cypriot Copper Alloy Artefacts.” *Journal of Archaeological Science: Reports* 7:566–73. Retrieved

(http://dx.doi.org/10.1016/j.jasrep.2015.12.010).

Charalambous, Andreas, Vasiliki Kassianidou, and George Papasavvas. 2014. “A Compositional Study of Cypriot Bronzes Dating to the Early Iron Age Using Portable X-Ray Fluorescence Spectrometry (PXRF).” *Journal of Archaeological Science* 46(1):205–16.

Comelli, Daniela et al. 2016. “The Meteoritic Origin of Tutankhamun’s Iron Dagger Blade.” *Meteoritics and Planetary Science* 51(7):1301–9.

Condamin, J. and M. Picon. 1964. “THE INFLUENCE OF CORROSION AND DIFFUSION ON THE PERCENTAGE OF SILVER IN ROMAN DENARII.” *Archaeometry* 7(1):98–105.

Contu, E. 2008. *La Sardegna Preistorica e Nuragica*. Carlo Delfino editore. Retrieved (https://books.google.it/books?id=XOaiAQAACAAJ).

Cosano, Daniel et al. 2018. “Spectroscopic Analysis of Corrosion Products in a Bronze Cauldron from the Late Iberian Iron Age.” *Spectrochimica Acta - Part A: Molecular and Biomolecular Spectroscopy* 205:489–96. Retrieved (https://doi.org/10.1016/j.saa.2018.07.072).

Craddock, P. T. 1976. “The Composition of the Copper Alloys Used by the Greek, Ertruscan and Roman Civilisations.” *Journal of Archaeological Science* 3(2):93–113.

Debernardi, Pierluigi et al. 2017. “Average and Core Silver Content of Ancient-Debased Coins via Neutron Diffraction and Specific Gravity.” *Archaeological and Anthropological Sciences* 1–18.

Depalmas, A. and Rita T. Melis. 2010. “The Nuragic People: Their Settlements, Economic Activities and Use of the Land, Sardinia, Italy.” in *Landscapes and Societies*, edited by I. P. Martini and W. Chesworth. Springer.

Dillmann, P., G. Béranger, P. Piccardo, and H. Matthiesen. 2007. *Corrosion of Metallic Heritage Artefacts: Investigation, Conservation and Prediction of Long Term*

Behavior. 1st ed. edited by P. Dillmann, G. Béranger, P. Piccardo, and H. Matthiesen. CRC Press.

Ferretti, M. 2000. "X-Ray Fluorescence Applications for the Study and Conservation of Cultural Heritage." Pp. 285–96 in *Radiation in Art and Archeometry*. Elsevier. Retrieved March 23, 2018 (http://linkinghub.elsevier.com/retrieve/pii/B9780444504876500596).

Figueiredo, Elin, M. Fátima Araújo, Rui J. C. Silva, and Raquel Vilaça. 2013. "Characterisation of a Proto-Historic Bronze Collection by Micro-EDXRF." *Nuclear Instruments and Methods in Physics Research, Section B: Beam Interactions with Materials and Atoms* 296:26–31. Retrieved (http://dx.doi.org/10.1016/j.nimb.2012.11.019).

Figueiredo, Elin, Rui J. C. Silva, M. Fátima Araújo, and Francisco M. Bra. Fernandes. 2013. "Multifocus Optical Microscopy Applied to the Study of Archaeological Metals." *Microscopy and Microanalysis* 19(5):1248–54.

Gallin, Lenore J. and Robert H. Tykot. 1993. "Metallurgy at Nuraghe Santa Barbara (Bauladu), Sardinia." *Journal of Field Archaeology* 20(3):335. Retrieved (http://www.tandfonline.com/doi/full/10.1179/jfa.1993.20.3.335%5Cnhttp://www.jstor.org/stable/530057?origin=crossref).

Golosio, Bruno, Tom Schoonjans, Antonio Brunetti, Piernicola Oliva, and Giovanni Luca Masala. 2014. "Monte Carlo Simulation of X-Ray Imaging and Spectroscopy Experiments Using Quadric Geometry and Variance Reduction Techniques." *Computer Physics Communications* 185(3).

Van Grieken, R. E. and a a Markowicz. 2002. *Handbook of X-Ray Spectrometry*. Second. edited by R. E. Van Grieken and A. A. Markowicz. Marcel Dekker, Inc. Retrieved (http://pubs.acs.org/doi/abs/10.1021/ac800678s).

Guerra, Maria Filomena. 2000. "The Study of the Characterisation and Provenance of Coins and Other Metalwork Using XRF, PIXE and Activation Analysis." Pp. 378–416

in *Radiation in Art and Archeometry*. Elsevier. Retrieved March 23, 2018 (http://linkinghub.elsevier.com/retrieve/pii/B9780444504876500638).

Harrison, A. and E. Howe. 2017. "Evidence of Soldering Technology on Pre-Columbian Gold Pendants from Western and North-Western Colombia." *Archaeometry* Online adv(June 2016):1–17. Retrieved (http://doi.wiley.com/10.1111/arcm.12286).

Hingston, J. .., C. .. Collins, R. .. Murphy, and J. .. Lester. 2001. "Leaching of Chromated Copper Arsenate Wood Preservatives: A Review." *Environmental Pollution* 111(1):53–66. Retrieved August 22, 2018 (https://www.sciencedirect.com/science/article/pii/S0269749100000300).

Ingo, G. M. et al. 2006. "Large Scale Investigation of Chemical Composition, Structure and Corrosion Mechanism of Bronze Archeological Artefacts from Mediterranean Basin." *Applied Physics A: Materials Science and Processing* 83(4):513–20.

Ingo, Gabriel M. et al. 2013. "Gold Coated Copper Artifacts from the Royal Tombs of Sipán (Huaca Rajada, Perù): Manufacturing Techniques and Corrosion Phenomena." *Applied Physics A: Materials Science and Processing* 113(4):877–87.

Kienlin, T. L., E. Bischoff, and H. Opielka. 2006. "Copper and Bronze during the Eneolithic and Early Bronze Age: A Metallographic Examination of Axes from the Northalphine Region." *Archaeometry* 48(3):453–68.

Knapp, Bernard A. 1990. "Ethnicity, Entrepreneurship, and Exchange: Mediterranean Inter-Island Relations in the Late Bronze Age." *The Annual of the British School at Athens* 85(September 2013):115–53.

Knapp, Bernard A. 2000. "Archaeology, Science-Based Archaeology and the Mediterranean Bronze Age Metals Trade." *European Journal of Archaeology* 3(1):31–56.

Knoll, Glenn F. 2010. *Radiation Detection and Measurement*. 4th ed. Wiley.

Lilliu, Giovanni. 2008. *Sculture Della Sardegna Nuragica*. I. Nuoro: Ilisso.

Loureiro, J. et al. 2014. “ESTUDO ARQUEOMETALÚRGICO DO CONJUNTO METÁLICO DO SÍTIO ARQUEOLÓGICO DE MOINHOS DE GOLAS (MONTALEGRE, NORTE DE PORTUGAL): PRIMEIROS RESULTADOS.” *Estudos Do Quaternário* 11:59–66.

Lukyanov, A. et al. 2014. “Microstructure Refinement in Cu-Fe Alloy Using High Pressure Torsion.” *IOP Conference Series: Materials Science and Engineering* 63(1):12102. Retrieved (http://stacks.iop.org/1757-899X/63/i=1/a=012102).

Manso, M. et al. 2015. “Alloy Characterization of a 7th Century BC Archeological Bronze Vase - Overcoming Patina Constraints Using Monte Carlo Simulations.” *Spectrochimica Acta - Part B Atomic Spectroscopy* 107:93–96. Retrieved (http://dx.doi.org/10.1016/j.sab.2015.03.001).

Mantovani, Luciana, Mario Tribaudino, and Grazia Facchinetti. 2016. “A Mineralogical Approach to the Authentication of an Archaeological Artefact: Real Ancient Bronze from Roman Age or Fake?” *Journal of Cultural Heritage* 21:876–80. Retrieved (http://dx.doi.org/10.1016/j.culher.2016.04.002).

Meeks, Nigel. 1993. “Surface Characterization of Tinned Bronze, High-Tin Bronze, Tinned Iron and Arsenical Bronze.” Pp. 247–75 in *Metal Plating and Patination*. Butterworth-Heinemann Ltd. Retrieved (http://linkinghub.elsevier.com/retrieve/pii/B978075061611950025X).

Melis, Paolo. 2003. *The Nuragic Civilisation*. A.G.E. Rome.

Minoja, M., G. Salis, and L. Usai. 2015. *L’isola Delle Torri: Giovanni Lilliu e La Sardegna Nuragica : Catalogo Della Mostra, Cagliari, 15 Marzo-30 Settembre, Roma, 28 Novembre 2014-7 Aprile 2015, Milano, 6 Maggio 2015-14 Febbraio 2016*. Carlo Delfino editore. Retrieved (https://books.google.it/books?id=3kRljwEACAAJ).

Moravetti, Alberto et al. 2014. *La Sardegna Nuragica : Storia e Materiali*. Delfino Carlo Editore.

Nascimento Filho, Virgílio F. 1999. “Técnicas Analíticas Nucleares de Fluorescência de

Raios x Por Dispersão de Energio (ED-XRF) e Por Reflexão Total (TXRF).” 32.

Nørgaard, Heide Wrobel. 2017. “Portable XRF on Prehistoric Bronze Artefacts: Limitations and Use for the Detection of Bronze Age Metal Workshops.” *Open Archaeology* 3(1):101–22. Retrieved (http://www.degruyter.com/view/j/opar.2017.3.issue-1/opar-2017-0006/opar-2017-0006.xml).

Paparazzo, Ernesto. 1994. “Surface and Interface Analysis of a Roman Lead Pipe ‘Fistula’: Microchemistry of the Soldering at the Join, as Seen by Scanning Auger Microscopy and X-Ray Photoelectron Spectroscopy.” *Applied Surface Science* 74(1):61–72.

Pillay, A. E., C. Punyadeera, L. Jacobson, and J. Eriksen. 2000. “Analysis of Ancient Pottery and Ceramic Objects Using X-Ray Flourescence Spectrometry.” *X-Ray Spectrometry* 29(May 1999):53–62.

Pronti, Lucilla et al. 2015. “Characterisation of Corrosion Layers Formed under Burial Environment of Copper-Based Greek and Roman Coins from Pompeii.” *Applied Physics A: Materials Science and Processing* 121(1):59–68.

Quaranta, Marta, Emilio Catelli, Silvia Prati, Giorgia Sciutto, and Rocco Mazzeo. 2014. “Chinese Archaeological Artefacts: Microstructure and Corrosion Behaviour of High-Leaded Bronzes.” *Journal of Cultural Heritage* 15(3).

Riederer, Josef. 1980. “Metallanalysen Sardischer Bronzen.” Pp. 156–60 in *Kunst Sardiniens*. Badisches Landesmuseum.

Robbiola, L., J. M. Blengino, and C. Fiaud. 1998. “Morphology and Mechanisms of Formation of Natural Patinas on Archaeological Cu-Sn Alloys.” *Corrosion Science* 40(12):2083–2111.

Schiavon, Nick, Angela Celauro, Marta Manso, Antonio Brunetti, and Fiammetta Susanna. 2013. “Iron-Age Bronze Statuettes in Southern Portugal: Combining Archaeological Data with EDXRF and BSEM + EDS to Assess Provenance and Production Technology.” *Applied Physics A: Materials Science and Processing* 113(4):865–75.

Schiavon, Nick, Anna de Palmas, Claudio Bulla, Giampaolo Piga, and Antonio Brunetti. 2016. “An Energy-Dispersive X-Ray Fluorescence Spectrometry and Monte Carlo Simulation Study of Iron-Age Nuragic Small Bronzes (‘Navicelle’) from Sardinia, Italy.” *Spectrochimica Acta - Part B Atomic Spectroscopy* 123:42–46. Retrieved (http://dx.doi.org/10.1016/j.sab.2016.07.011).

Schoonjans, Tom et al. 2012. “A General Monte Carlo Simulation of Energy Dispersive X-Ray Fluorescence Spectrometers - Part 5: Polarized Radiation, Stratified Samples, Cascade Effects, M-Lines.” *Spectrochimica Acta - Part B Atomic Spectroscopy* 70:10–23. Retrieved (http://dx.doi.org/10.1016/j.sab.2012.03.011).

Schoonjans, Tom. 2012. “Three Dimensional Quantitative X-Ray Fluorescence at the Micro- and Nanoscopic Level: Methodological Development and Applications.” Universiteit Gent.

Scott, David A. 2002. *Copper and Bronze in Art*. J. Paul Getty Trust.

Selwyn, Lyndsie. 2004. *Metals and Corrosion: A Handbook for the Conservation Professional*. Canadian Conservation Institute.

Da Silva, Marialina S. 2017. “Análise Multielementar Por EDXRF Em Amostras de Solo de Região Agrícola de Duas Barras.” Universidade do Estado do Rio de Janeiro.

Stos-Gale, Z. A., G. Maliotis, N. H. Gale, and N. Aannets. 1997. “Lead Isotope Characteristics of the Cyprus Copper Ore Deposits Applied To Provenance Studies of Copper Oxhide Ingots.” *Archaeometry* 39(1):83–123. Retrieved (http://doi.wiley.com/10.1111/j.1475-4754.1997.tb00792.x).

Vincze, Laszlo, Koen Janssen, and Fred Adams. 1993. “A General Monte Carlo Simulation of Energy-Dispersive X-Ray Fluorescence Spectrometers-I. Unpolarized Radiation, Homogeneous Samples.” *Spectrochimica Acta Part B: Atomic Spectroscopy* 48(4):553–73.

Webster, Gary S. 1991. “Monuments, Mobilization and Nuragic Organization.” *Antiquity* 65:840–56.

Webster, Maud. 2014. “Water-Temples of Sardinia: Identification, Inventory and Interpretation.” Uppsala Universitet. Retrieved (http://uu.diva-portal.org/smash/get/diva2:760470/FULLTEXT01.pdf).

Zschornack, G. 2007. *Handbook of X-Ray Data*. Springer Berlin Heidelberg.

APPENDEX

ANNEX A

N. Inv.	Object	Description	Spots analyzed	Photo	Dimensions
24_42	Dagger 42	Dagger blade presenting 5 holes at the hilt	P1 and P2: central part, one at each blade side P3 and P4: hilt, one at each side		Weight: 48.65 g Length. 14.6 cm Width. 4.1 cm Thickness: 0.1 cm (blade) 0.3 cm (tang)
24_43	Dagger 43	Dagger blade	P1: area immediately below the tip P2: medium point P3: hilt	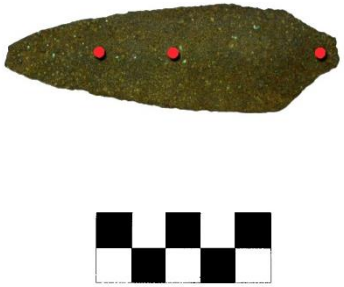	Weight: 18.17 g Length: 9.7 cm Width: 3.2 cm Thickness: 0.2 cm

24_44	Dagger 44	Triangular dagger blade with pin	P1: tip P2: central part		Weight: 18.34 g Length. 7.3 cm Width. 3.0 cm Thickness. 0.3 cm Ledge diameter: 0.3 cm
24_47	*Bronzetto* 47	Anthropomorphic figurine of an archer	P1: right arm, oxidized spot P2: right arm, no clear sign of encrustation or heavy corrosion P3: kilt medium point		Weight: 64,97 g Height: 7.2 cm (ankle-arch) 6.5 cm (body only) Width: 2.5 cm Thickness: 3.7 cm

24_49	*Navicella*	Small boat replica	P1: left side P2: left side, oxidized (or encrusted) spot P3: bottom		Weight: 247.77 g Length. 15.2 cm Width. 4.4 cm Height. 12.5 cm
24_52	*Bronzetto* 52	Anthropomorphic figurine of an archer	P1: kilt in the pelvis area. Front side P2: left rib P3:left leg, spot immediately below the knee		Weight: 95.48 g Height: 9.9 cm Width: 3.0 cm 1.4 cm (hips)

110	Double axe "*axe-adze*"	Double axe with orthogonal edges	P1 and P2: flat edge, both sides. P3: handle insert area P4: cutting edge		Weight: 108.35 g Length: 10.7 cm Width: 2.6-3.1 cm Height: 1.5-2.7 cm
111	Axe	Axe with raised cutting edges	P1 and P2: mid-point of the axe, one at each side P3 and P4: cutting edge of the axe, one at each side		Weight: 226,05 g Length: 10,7 cm Width: 2.6-4.3 cm Thickness: 1.5-1.0 cm

114	Boat head	Deer head usually inserted on the tip of Navicella models. It is missing the left antler	P1: nose tip P2: right antler, outer side		Weight: 49.20 g Length. 3.9 cm Width 2.6 cm Height: 5.5 cm Neck diam.: 0.7 cm Internal hole diam.: 0.4 cm

ANNEX B

```
# Lib import.
import numpy as np
import math

# Reads a vector in .txt format (one entry per line).
def read(input_):
    # open file and get data
    with open(input_) as f:
        data = f.readlines()
    # close file
    f.close()
    return data

# Chi-squared test between two compatible vectors.
def Qquad(v1,v2):
    return math.sqrt(np.sum((v1-v2)**2))/len(v1)

# Read simulated data.
x = np.array(read('x.txt'), dtype=float)
y = np.array(read('y.txt'), dtype=float)

# Read experimental data.
exp_x = np.array(read('x_.txt'), dtype=float)
exp_y = np.array(read('y_.txt'), dtype=float)


# Translates the experimental data:

#  Initialize vectors of zeroes x_ e y_
x_ = np.zeros(len(x),dtype=float)
y_ = np.zeros(len(y),dtype=float)

select = 0; # search optimization variable.

#  Run simulated X axis.
for i in range(len(x)):
    dif = 1000    # Run experimental x_ to find the closest matching value to the
simulated x and
    #  attributes values to x_ and y_ accordingly.
    for j in range(select, len(exp_x)):
        if dif > abs(exp_x[j] - x[i]):
            x_[i] = exp_x[j];
            y_[i] = exp_y[j];
            dif = abs(exp_x[j] - x[i])
            select = j
        else:
            break;

# Display chi-squared result between simulated x and y values and x_ and y_
experimental values.
print("Qquad (X, X_) = " + str(Qquad(x,x_)))
print("Qquad (Y, Y_) = " + str(Qquad(y,y_)))
```

ANNEX C

Spot	N. Inv.	Object	Composition							Patina thick. (µm)	Impurities	Chi²-test
			Cu	Sn	Pb	Fe	Zn	As	Others			
1	24_42	Dagger 42	73.40	17.20	3.90	1.00	0.20	2.70	1.60	27	Ag + Ni + Sb	8.6
2			79.65	13.30	2.90	0.60	0.20	2.30	1.05	38	Ag + Ti + Ni + Sb	12.2
3			83.10	9.30	4.10	0.50	0.20	2.10	0.70	34	Ag + Ni + Sb	13.5
4			73.55	19.95	3.30	0.25	0.20	1.85	0.90	24	Ag + Bi + Ni + Sb	8.5
1	24_43	Dagger 43	71.85	18.00	5.95	2.50	0.20	1.50	-	32		7.6
2			70.55	19.40	5.25	2.40	0.20	2.20	-	33		7.8
3			82.10	9.20	5.20	1.80	0.20	1.50	-	31		11.2
1	24_44	Dagger 44	71.20	18.20	9.10	0.20	-	1.20	0.10	26	Ni	7.0
2			69.30	20.20	9.20	0.20	-	1.00	0.10	34	Ni	7.3
1	24_47	*Bronzetto 47*	74.30	15.30	6.90	0.45	0.20	2.85	-	25		9.3
2			70.50	17.10	8.10	1.35	0.20	2.75	-	33		8.3
3			74.00	15.10	8.10	0.70	0.20	1.90	-	31		9.0
1	24_49	*Navicella*	71.40	3.40	9.00	9.60	6.00	-	0.60	98	Cr	11.4
2			73.85	5.50	10.15	1.30	9.10	0.10	-	96		14.4
3			83.10	3.40	4.50	3.20	5.00	-	0.80	110	Cr	13.2
1	24_52	*Bronzetto 52*	81.30	13.05	0.70	0.10	0.55	4.30	-	89		7.5
2			89.45	3.40	0.90	0.60	-	5.15	0.50	120	Cr	11.5
3			89.85	3.40	0.90	0.20	-	5.15	0.50	92	Cr	11.6
1	110	Double axe	82.65	7.90	4.80	0.25	-	4.40	-	82		10.1
2			87.70	5.10	3.00	0.10	-	4.10	-	94		17.6
3			85.87	6.60	4.10	0.33	-	3.10	-	82		7.8
4			78.40	11.10	5.50	0.60	-	4.40	-	72		7.5
1	111	Axe	79.10	7.40	3.40	10.10	-	-	-	60		13.0
2			76.65	13.90	2.85	5.40	-	0.15	1.05	62	Ti + Cr	9.4
3			84.30	10.40	1.50	3.80	-	-	-	67		11.1
4			77.80	14.00	3.80	3.20	-	1.20	-	62		9.9
1	114	Boat head	38.70	9.10	50.00	1.20	-	1.00	-	38		4.1
2			33.00	10.50	54.00	1.00	-	1.50	-	62		5.2